



Contents lists available at ScienceDirect

## Advances in Colloid and Interface Science

journal homepage: [www.elsevier.com/locate/cis](http://www.elsevier.com/locate/cis)

Historical perspective

## Linear viscoelasticity of complex coacervates

Yalin Liu, H. Henning Winter, Sarah L. Perry\*

Department of Chemical Engineering, University of Massachusetts Amherst, Amherst, MA 01003, USA

## ARTICLE INFO

Available online xxx

## Keywords:

Coacervate  
Rheology  
Viscoelasticity  
Small-Amplitude Oscillatory Shear  
Polyelectrolytes

## ABSTRACT

Rheology is a powerful method for material characterization that can provide detailed information about the self-assembly, structure, and intermolecular interactions present in a material. Here, we review the use of linear viscoelastic measurements for the rheological characterization of complex coacervate-based materials. Complex coacervation is an electrostatically and entropically-driven associative liquid–liquid phase separation phenomenon that can result in the formation of bulk liquid phases, or the self-assembly of hierarchical, microphase separated materials. We discuss the need to link thermodynamic studies of coacervation phase behavior with characterization of material dynamics, and provide parallel examples of how parameters such as charge stoichiometry, ionic strength, and polymer chain length impact self-assembly and material dynamics. We conclude by highlighting key areas of need in the field, and specifically call for the development of a mechanistic understanding of how molecular-level interactions in complex coacervate-based materials affect both self-assembly and material dynamics.

© 2016 Published by Elsevier B.V.

## Contents

1.	Introduction . . . . .	0
2.	A brief introduction to linear viscoelasticity . . . . .	0
3.	Connecting coacervate phase behavior with material dynamics . . . . .	0
3.1.	Viscosity . . . . .	0
3.2.	Frequency sweeps . . . . .	0
3.2.1.	Time–salt superposition . . . . .	0
3.2.2.	Time–pH superposition . . . . .	0
3.3.	Relaxation time spectra . . . . .	0
4.	Other applications of dynamics . . . . .	0
4.1.	Encapsulation and release . . . . .	0
4.2.	Gelation . . . . .	0
4.3.	Self-healing and structural recovery . . . . .	0
4.4.	Hierarchically-structured coacervate-based materials . . . . .	0
4.5.	Linear viscoelasticity <i>in vitro</i> and <i>in vivo</i> . . . . .	0
5.	A survey of materials rheology in complex coacervates . . . . .	0
6.	Perspective and future vision . . . . .	0
	Acknowledgements . . . . .	0
	References . . . . .	0

## 1. Introduction

Complex coacervation is an associative, liquid–liquid phase separation that results from the electrostatic interaction of oppositely charged macro-ions. The self-assembly of these materials is driven by entropy, where the initial electrostatic attraction between oppositely-charged

\* Corresponding author.  
E-mail address: [perryys@engin.umass.edu](mailto:perryys@engin.umass.edu) (S.L. Perry).

macro-ions results in the release of small, bound counter-ions and the restructuring of water molecules [1–4]. Complex coacervates have a long history of use in the food [5–13] and personal care [14,15] industries, and have found increasing utility as a platform for drug and gene delivery [1–4,16–47], as well as underwater adhesives [5–13,48–62]. Coacervation has also recently been implicated in the formation of various biological assemblies [1,14–16,55,63–70]. Across nearly all of these applications, the vast majority of studies have focused on understanding and characterizing the equilibrium phase behavior of these materials as a function of parameters such as the chemistry of the charged species, the charge stoichiometry of the system, ionic strength, and pH [1–3,17,69,71–116]. However, these types of equilibrium characterizations do not provide sufficient insight into the dynamic behavior of coacervates.

To access the dynamic response of a material over a variety of time-scales, small-amplitude oscillatory shear (SAOS) tests have become the canonical method. SAOS probes the linear viscoelastic properties of complex fluids and can provide information on material functions such as viscosity, modulus, and yield stress, along with more dynamic information, such as the characteristic timescales for molecular motion within a material [117–121]. These types of analyses can also be used to unambiguously identify the nature of solid-to-liquid transitions; for instance, distinguishing gelation as compared to a glass transition [122, 123]. The well-established theoretical backing of SAOS measurements also allows for the development of models to help test molecular and mechanistic hypotheses. This review is intended to provide an introduction to the use of rheology and linear viscoelasticity measurements for the characterization of complex coacervate-based materials in the context of reported work to date, much of which is focused on polymeric materials. In establishing this framework, we highlight the need for further systematic and detailed rheological characterization of complex coacervate-based materials to support the burgeoning renaissance of basic science and application-driven research in this area.

## 2. A brief introduction to linear viscoelasticity

While rheology relates to the study of the deformation and flow of materials in general, here we will limit our discussion to the linear viscoelastic behavior of complex coacervate-based materials through the use of small-amplitude oscillatory shear (SAOS) measurements. SAOS conditions are explicitly defined as a situation where the material functions are independent of the applied strain amplitude, resulting in a preservation of the structure of the material. Viscoelastic materials have a different mechanical response to an applied stress  $\sigma$  or strain  $\gamma^o$ , depending on the timescale of the measurement. For oscillatory shear measurements, this stress/strain response is defined in terms of two measured properties as a function of the oscillation frequency  $\omega$ . Most commonly, the viscoelastic response is described with respect to the storage (or elastic) modulus  $G'$ , and the loss (or viscous) modulus  $G''$ .

$$\frac{\sigma(\omega, t)}{\gamma^o} = G' \sin(\omega t) + G'' \cos(\omega t) \quad (1)$$

The storage modulus  $G'$  describes the “in-phase” response of the shear stress to a periodic shear strain of amplitude  $\gamma^o$  on the material (*i.e.*, effectively a cosinusoidal response), while the loss modulus  $G''$  describes the “out-of-phase” response, related to the ability of the material to dissipate energy (*i.e.*, a sinusoidal response). These two material functions can also be expressed in terms of a complex modulus  $G^*$  and the phase angle difference between the applied strain and the resultant stress  $\delta$ .

$$|G^*| = \sqrt{G'^2 + G''^2} \quad (2)$$

$$\tan(\delta) = \frac{G''}{G'} \quad (3)$$

One of the most important experimental considerations for SAOS measurements is to verify that the measured moduli are independent of the applied strain amplitude, or that the experimental conditions fall within the “linear regime.” Operation within the linear regime is necessary for Eqs. (1)–(3) to be valid. The limits of the linear viscoelastic regime are typically identified by performing a series of amplitude sweeps over the range of desired experimental frequencies. In these measurements, the amplitude of the shear stress is increased at a constant frequency until a decrease in the moduli  $G'$  and  $G''$  is observed, defining the limits of the linear regime. Subsequent experiments should then be performed using a shear stress that is valid within this region over the desired range of frequencies.

SAOS experiments are typically performed using a (i) parallel plate geometry, (ii) a cone-plate geometry, or (iii) an annular Couette cell in a rotational rheometer configuration. Experimentally, each of these three geometries has its own unique advantages and limitations. Here, we provide a brief introduction to these geometries, but refer the reader to the textbook by Macosko for further details [117]. The cone-plate geometry has the advantage of providing a homogeneous strain field, but requires a prescribed gap while the parallel plate arrangement can be operated at a range of plate separation distances. Thus, a parallel plate configuration might prove necessary for stiff samples, where the necessary gap height for a cone-plate arrangement cannot be met, or when small sample quantities are insufficient to fill the prescribed space in the rheometer. The homogeneous field of the cone-plate geometry is important in the context of non-Newtonian fluids such as complex coacervates, because for the inhomogeneous strain field resulting from a parallel plate geometry, the measured stress will be a convolution of the material response to the applied strain field, rather than a direct stress–strain measurement. Thus, when employing a parallel plate geometry, it is advisable to repeat the experiment using different sample thicknesses to ensure the robustness of the experiment. The Couette cell generates a homogeneous strain field and is capable of performing more sensitive measurements than either parallel plate or cone-plate configurations because of the increased surface area-to-volume ratio of the annular setup. However, the Couette cell requires large sample volumes. Finally, the sensitivity of the experimental geometry must be coupled with the operational strategy of the rheometer. Strain-controlled instruments are advantageous for softer materials that require more sensitive measurements by eliminating concerns related to the inherent inertia associated with the motion of the instrument itself.

## 3. Connecting coacervate phase behavior with material dynamics

Experimentally, complex coacervate samples are typically prepared by mixing aqueous solutions of oppositely-charged macro-ions. The resulting phase separation causes the sample to take on a cloudy, or opalescent appearance, due to the formation of small droplets of the complex coacervate phase (Fig. 1). Characterization of coacervate phase behavior is typically performed using methods that take advantage of the light scattered by these small droplets in solution, such as turbidity and/or light scattering. While rheology can be used to identify the advent of complex formation based on an increase in viscosity [124], optical methods have been more widely utilized because they are amenable for high-throughput analysis to quantify the impact of variables such as the charge stoichiometry of the mixture, the ionic strength and pH of the solution, the total concentration of macro-ions, the charge density, and for samples containing polyelectrolytes, the polymer molecular weight [1–3,17,69,71–116].

The qualitative nature of turbidity-style measurements allows a phenomenological characterization of coacervate phase behavior, rather than a more direct quantification of the binodal phase space [8,15,71,73–77,83,88,91–93,104,105,108,112,114,125–153]. Typical characterization experiments include evaluation of the stoichiometric ratio of polycation to polyanion, the effect of increasing salt concentration,

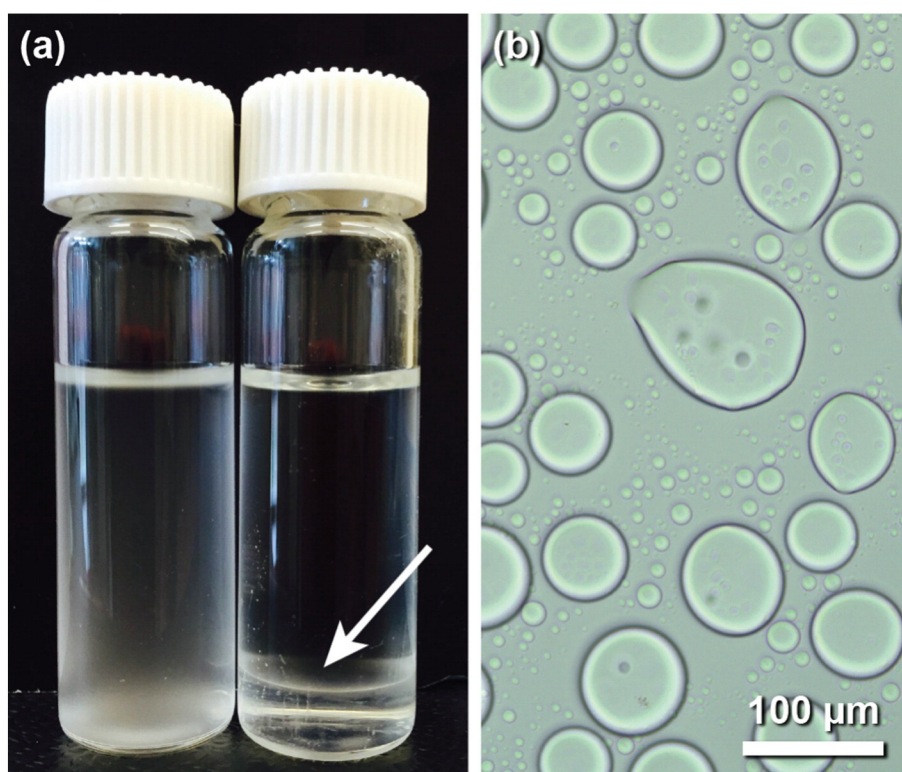


**Fig. 1.** Images of complex coacervates formed from poly(diallyldimethyl ammonium chloride) (PDADMAC) and poly(styrene sulfonate sodium salt) (PSS) in 1.6 M KBr. (a) A photograph of a typical opalescent dispersion of coacervate droplets (left) and the dense, coalesced coacervate phase (right, indicated by arrow) in equilibrium with the aqueous supernatant. (b) An optical micrograph of the dispersion of liquid coacervate droplets from (a), settled onto a glass slide.

and the effect of variable pH. An example of these types of turbidimetric data for a system of poly(acrylic acid sodium salt) (PAA) and poly(allylamine hydrochloride) (PAH) is shown in Fig. 2. The presence or absence of coacervation can be inferred from the intensity

of the turbidity readings. However, quantitative information about the composition of the coacervate phase or the extent of phase separation is unknown, as is information relating to the viscosity or other material properties. For instance, in Fig. 2a, coacervation in the absence of added

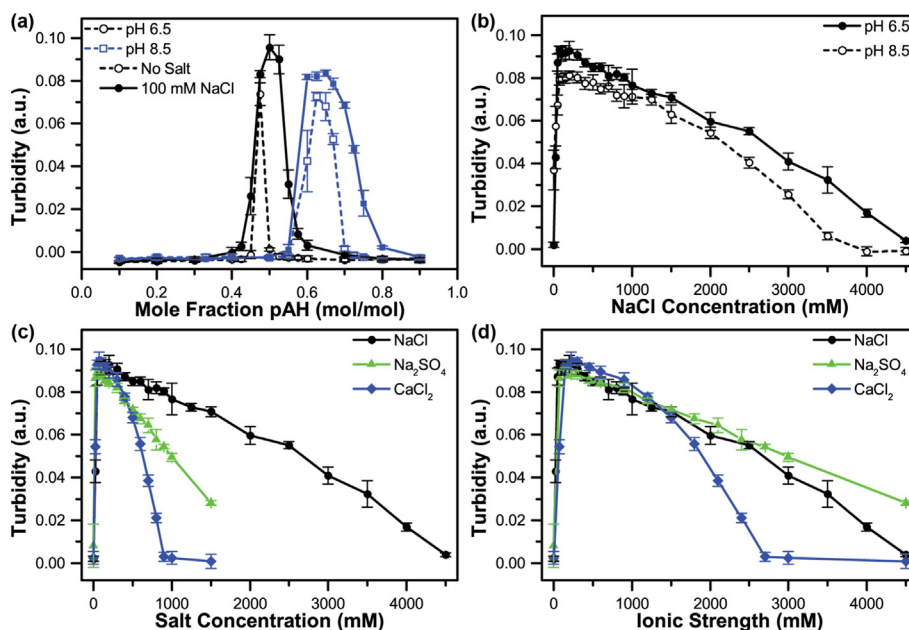


**Fig. 2.** (a) Plot of turbidity as a function of the mole fraction of the number of charges contributed by the polycation PAH in complex with PAA at pH 6.5, where both polymers are fully charged (black circles) and pH 8.5 where PAH is only half-charged (blue squares). Data are shown for conditions of no salt (open symbols) and 100 mM NaCl (closed symbols). (b) Turbidity as a function of NaCl concentration at pH 6.5 where both polymers are fully charged (closed) and pH 8.5 where the PAH is half-charged (open). All samples were prepared at charge-neutral conditions (50/50 mol% PAA/PAH at pH 6.5 and 33/67 mol% PAA/PAH at pH 8.5). Plots of turbidity as a function of (c) salt concentration and (d) ionic strength for a selection of monovalent and divalent salts for samples were prepared at 50/50 mol% PAA/PAH ratio at pH 6.5. All samples were prepared at 1 mM total monomer concentration.

Figures adapted with permission from Ref. [77] (Perry et al., *Polymers*, (2014), 6, 1756–1772).

salt occurs over a narrow range of polymer compositions. For the case of two fully charged polymers (pH 6.5) with the same molecular weight, this peak occurs at a 50/50 mixture of PAH to PAA. Similarly, this peak shifts to a composition of 67/33 PAH/PAA at a pH of 8.5, where PAH is only half charged. The addition of 100 mM NaCl serves to broaden the range of compositions over which coacervation is observed. While intuition suggests that it is reasonable for a coacervate formulation to prefer compositions which satisfy electroneutrality, it is important to emphasize that turbidity observations are connected only with the knowledge of the initial sample formulation, and do not correspond in any way to the actual composition of the final coacervate mixture.

We further highlight the issue of composition as compared to phenomenological observations with respect to the effect of added salt. Turbidimetric analysis of the impact of increasing NaCl concentration on both the optimal 50/50 PAH/PAA at pH 6.5, and the 67/33 PAH/PAA sample at pH 8.5 shows a sharp increase in the turbidity signal with the addition of small amounts of salt, followed by a slow loss of signal at higher salt concentrations. Finally, a critical salt concentration is reached, above which no coacervation is observed (Fig. 2b) [77]. The turbidity measurements demonstrate a difference in the critical salt concentration for samples prepared at the two different pH conditions. However, these data do not provide information on whether the observed changes in turbidity correspond to differences in the coacervate droplet number, size, water content, or the overall coacervate yield. Similarly, in the case where the effect of different salts is investigated, there is no way to parse whether the presence of divalent salts leads to a change in coacervate composition due to disproportionation, an increase in coacervate stiffness due to crosslinking by divalent ions, a

change in water content due to differences in osmotic pressure, or other unanticipated effects.

While turbidity experiments do not provide direct, quantitative data relating to coacervate composition, such experiments can be used to quantitatively map out binodal curves. The critical missing parameter needed to connect observations of phase separation and a phase diagram is the concentration of the various species in each phase. However, for a given composition and overall concentration of macro-ions, turbidity can be utilized to identify the critical salt concentration which defines the phase boundary. At this point, where phase separation is no longer observed, one can reasonably take the composition of the very last miniscule droplet of coacervate phase to equal that of the overall sample – defining a single point on the binodal curve. Alternatively, direct measurements of the macro-ion and salt composition in both the dilute and coacervate phases can be performed.

An example of these types of detailed binodal curves is shown in Fig. 3 for the system of poly(acrylic acid) (PAA) in complex with poly(*N,N*-dimethylaminoethyl methacrylate) (PDMAEMA), in the presence of KCl [78]. The phase behavior of this system was analyzed only for a 1:1 stoichiometric (charge-neutral) mixture of PAA and PDMAEMA, rather than for the entire range of PAA-PDMAEMA-KCl composition space depicted in Fig. 3b. Quantification of the PAA concentration in the two phases was achieved using fluorescein-tagged PAA (Fig. 3a), with the authors using a simplifying assumption that the concentration of salt in the two phases was equal to the overall concentration. The data shown in Fig. 3c demonstrates a broadening of the two-phase region with increasing degree of polymerization. The binodal curves also show that increasing salt concentration decreases

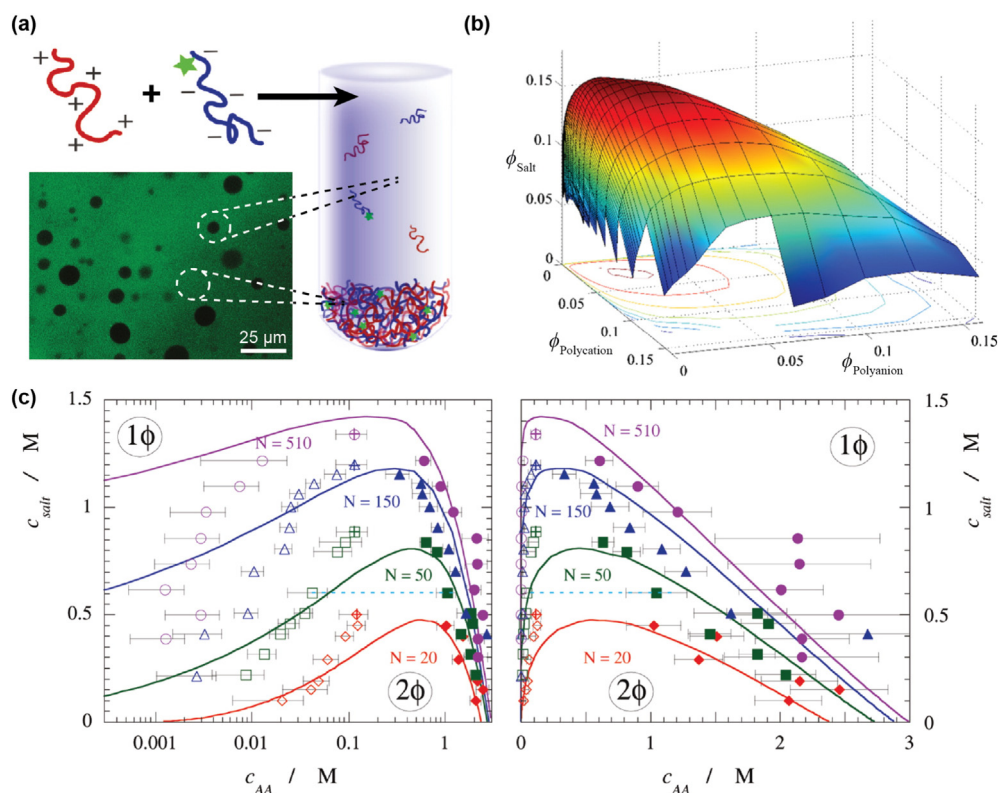


**Fig. 3.** (a) Schematic depiction of the formulation of fluorescently labeled coacervates using fluorescein-labeled PAA in complex with PDMAEMA. The confocal fluorescence micrograph shows an equilibrated mixture of the brightly fluorescent coacervate phase of PAA and PDMAEMA with droplets of coexisting dilute phase. (b) Three-dimensional representation of a phase diagram for polyelectrolyte complexation calculated using the theory of Voorn and Overbeek [163]. Points below the drawn surface are unstable and result in phase separation where compositions are dictated by the phase equilibrium. (c) Experimentally measured phase diagrams depicting the binodal curve for coacervation between stoichiometric (1:1) mixtures of PAA and PDMAEMA at pH 6.5 in the presence of KCl on a logarithmic scale (left) and a linear scale (right). Solid lines are theoretical predictions of the phase behavior generated using the Voorn–Overbeek theory.

Figures (a) and (c) adapted with permission from Ref. [78] (Spruijt et al., *Macromolecules*, (2010), 43, 6476–6484). Copyright 2010 American Chemical Society. Figure (b) adapted from Ref. [1] (van der Gucht et al., *J. Coll. Interf. Sci.*, (2011), 361, 407–422) with permission from Elsevier.

the concentration of polymer present in the dense, coacervate phase while having a minimal effect on the concentration of polymer present in the dilute phase. These trends have been presented in a visually dramatic fashion through a comparison of macro-phase separated samples prepared at constant overall polymer composition and increasing salt concentration for a system of PSS with PDADMAC (Fig. 4). The measured decreases in polymer concentration can clearly be seen as an increase in the water content of the sample. Similar trends have been observed in a variety of other systems, [1,71,73,74,76,77,81–83,85,87,92,94,105,127,128,132,143,154–162], and have also been predicted from theory [75,78,156,163–170].

### 3.1. Viscosity

While binodal curves elucidate the compositional aspects of complex coacervation, the next critical level of understanding focuses on understanding of how the observed trends in composition relate to dynamic material properties. This type of mechanical characterization can give insight into the molecular-level interactions present in the material, and is critical to enable effective processing of these materials. Generally, coacervates have been reported to have a Newtonian, or a shear-rate independent viscosity [71,111,171,172], as well as a shear thinning response [2,87,111,124,171–175], depending on the shear rate. The occurrence of shear thinning is suggestive of a structural change in the material, and research has suggested that the tendency for shear thinning in coacervate-based materials may correlate with the strength of the underlying electrostatic interactions [2,174]. For example, in coacervates formed from whey proteins and gum Arabic, pH was used to modulate the strength of the electrostatic interactions. A correlation was observed between the degree of shear thinning and the sample pH. More significant shear thinning was observed for samples where the pH facilitated stronger electrostatic interactions between the coacervate components. However, in all cases the initial viscosity and shear response of the sample could be recovered, given sufficient recovery time relative to the relaxation times for the material, showing that the structural changes were reversible.

Recalling the coacervate system composed of PDMAEMA and PAA in KCl, Fig. 3 showed that increasing salt concentration decreases the concentration of polymer present in the coacervate phase by increasing the amount of water present. Rheological characterization demonstrated that these trends correlate with decreasing coacervate viscosity with increasing salt concentration (Fig. 5a) [71,79,157]. Furthermore, the viscosity was seen to increase as a function of degree of polymerization (Fig. 5b) [79], as would be expected for polymeric materials. Inspection of the data in Fig. 5 suggests that viscosity varies exponentially with salt

concentration, and follows a power-law behavior as a function of polymer chain length. Interestingly, no change in viscosity was observed as a function of PDMAEMA/PAA stoichiometry, suggesting that the coacervate may undergo disproportionation to maintain a charge-neutral ratio of the two polymers [79].

Spruijt et al. proposed a model for these rheological observations based on “sticky” Rouse (or Zimm) polymer dynamics, where ionic bonds between polyelectrolyte chains act as “sticky” points that enhance the effective friction of polymer chains and decrease their mobility, thus slowing down stress relaxation [79,111]. This model provides a platform for developing and testing our understanding of molecular-level interactions within the material, and reasonable agreement was obtained between the model and the data. For instance, the model predicts a power-law relationship between zero-shear viscosity and polymer length, as observed by the linear trend in the log–log plot (Fig. 5b). This type of power-law dependence is expected for linear homopolymers, with a slope of 1 at short chain lengths, and a slope of 3.4–3.5 above the critical molecular weight for entanglement [117,118,120]. The data shown in Fig. 5b show a decrease in the observed slope from ~2.2 at low salt to ~1.4 at high salt concentrations, suggesting that complexation between chains within the coacervate alters the expected molecular weight dependence. The model also predicts an exponential relationship between zero-shear viscosity and the square root of the salt concentration. The semi-log plot in Fig. 5a shows a linear trend in the data, suggesting agreement with the exponential trends. However, further testing and validation of the model would benefit from systematic characterization of additional model polymer systems.

### 3.2. Frequency sweeps

Moving beyond simple consideration of viscosity, the frequency response of coacervate-based materials has been studied as a function of numerous variables, including salt concentration, pH, stoichiometry, and the presence of guest molecules. By analyzing the in-phase and out-of-phase response of a material, frequency sweep data provides a characterization of the response over a range of different timescales. A schematic depiction of the characteristic response of a polymer solution is shown in Fig. 6. At the lowest frequencies (i.e., in the terminal region), the loss modulus ( $G''$ ) dominates over the storage modulus ( $G'$ ), indicating a viscoelastic liquid-like behavior. In the terminal region, the storage modulus ( $G'$ ) shows a power-law slope of 2, while the loss modulus ( $G''$ ) shows a power-law slope of 1. At higher frequencies, a crossover in the two moduli is observed, which extends into a plateau region where rubbery behavior arises, followed ultimately by a region where glassy, solid-like behavior dominates [118,120,176].

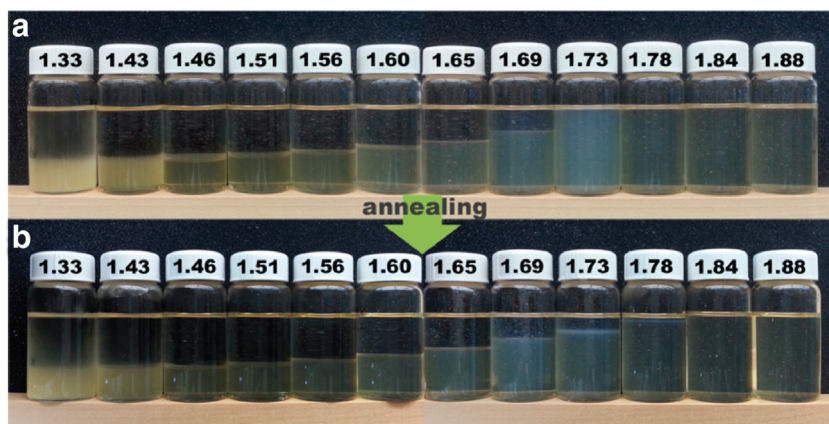


**Fig. 4.** Photographs of (a) as-prepared PSS/PDADMAC coacervate samples stored for 30 days and (b) the samples 10 days after annealing for about 3 h at 60 °C and cooled to room temperature. The numbers indicate the concentration of KBr (in M) for each sample. Increasing water content is observed in the coacervate phase up to 1.80 M KBr, above which, only a single solution phase is observed.

Figure adapted with permission from Ref. [157] (Wang and Schlenoff, *Macromolecules*, (2014), 47, 3108–3116). Copyright 2014 American Chemical Society.

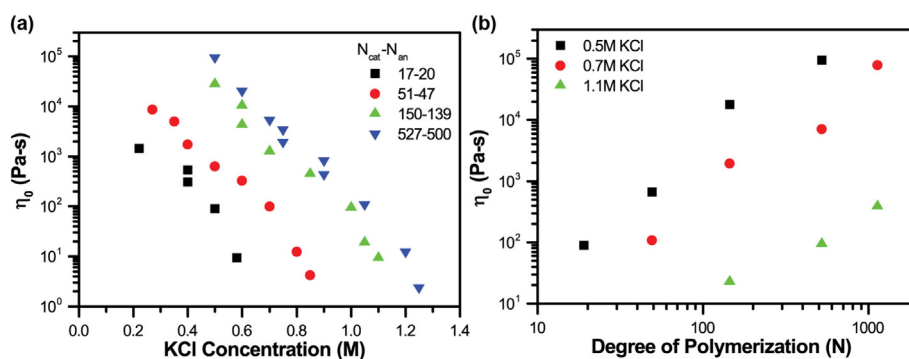


**Fig. 5.** (a) Zero shear viscosity ( $\eta_0$ ) vs. overall KCl concentration for coacervates of different chain lengths. The linear trend observed on a semi-log plot is indicative of an exponential behavior with respect to salt concentration. (b) Zero shear viscosity ( $\eta_0$ ) vs. the average polymer length (N) for coacervates formed at different overall concentrations of KCl. The linear trend on the log–log plot is indicative of a power law trend with respect to N. Data are for stoichiometric (1:1) PDMAEMA/PAA coacervates formed in the presence of varying concentrations of KCl, pH 6.5.

Figures adapted with permission from Ref. [79] (Spruijt et al., *Macromolecules*, (2013), 46, 1633–1641). Copyright 2013 American Chemical Society.

Interestingly, complex coacervates have been reported with dramatically different material properties. In numerous examples, the elastic behavior dominates (*i.e.*, the storage modulus ( $G'$ ) dominates) [8,61,137,138,171,175,177–180], while in other coacervates the viscous or liquid-like behavior (*i.e.*, the loss modulus ( $G''$ ) dominates) [95,103,171]. Meanwhile, there are other systems where a crossover is observed between the two regimes, with  $G''$  dominating at low frequencies, and  $G'$  dominating at higher frequencies [61,71,72,79,111,130,162,171]. Considering these observations in the context of the expected characteristic responses for polymeric materials suggests that the differences in the observed material properties are the result of experimental limitations and thermodynamic factors that limit experimental access to the full range of frequency behavior, rather than an inherent characteristic of the material itself. In general, the trends observed in frequency sweep data parallel those for viscosity, due to the relationship between dynamic viscosity and modulus. In general, increasing salt concentration leads to a decrease in both the storage and loss modulus (Fig. 7a) [71,75,79]. Similarly, changes in pH that weaken the electrostatic interactions between polymer chains also decrease the moduli (Fig. 7b) [75]. Increasing polymer chain length, on the other hand causes an increase in modulus and viscosity due to an increased propensity for entanglements, up to an asymptotic limit for an infinitely long polymer chain (Fig. 8) [79].

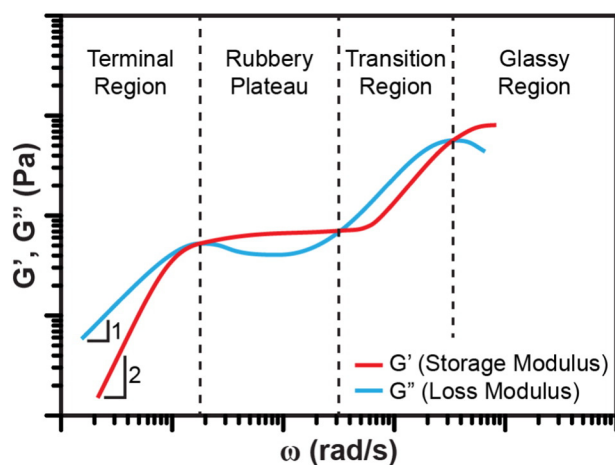


**Fig. 6.** Schematic depiction of the viscoelastic behavior for polymer solutions as a function of frequency, showing the terminal behavior of the storage and loss moduli at low frequency (with indicated slope), the rubbery plateau, transition region, and final glassy region at high frequency. The logarithmic indicators on the axes are for visualization purposes only.

The crossover frequency, defining the transition from the terminal region to the rubbery plateau region, has also been observed to shift as a function of salt, pH, and polymer chain length. The inverse of the frequency of this crossover point relates to the longest relaxation time for the polymers in the sample, or the time necessary for the polymer molecules to disentangle. Thus, the observation of decreasing crossover frequency for increasing polymer chain length (Fig. 8) corresponds to an increase in the time needed for longer polymer molecules to disentangle and relax. Intriguingly, Spruijt et al., reported significant differences in the rheological response for coacervates formed from PAA and PDMAEMA with mismatched polymer chain lengths depending on whether the asymmetry was applied to the length of the polycation or the polyanion [79]. When the length of the cationic PDMAEMA was decreased relative to the PAA, the expected decrease in moduli was observed and the crossover point shifted to higher frequencies. However, when the inverse experiment was done, the viscoelastic response of the material remained almost constant. The question of whether the dynamics of complex coacervates are dominated by the chain length of the polycation, and perhaps its interactions with water, or whether this observed behavior could be affected by different polymer chemistries remains an open question.

Similar to chain length effects, the argument could also be made that a weakening in the electrostatic interactions between coacervate components, via salt (and the subsequent increase in water content), should also lead to a decrease in this timescale by lowering friction between molecules and allowing for faster relaxation. Data supportive of this hypothesis has been reported by various groups [61,79,103]. However, the opposite trend has also been reported. For example, reports by Pfriftis et al., have shown a decreasing trend in crossover frequency (*i.e.*, longer relaxation times) with increasing salt concentration (Fig. 7a) [71,75]. This difference in the dynamics of the various coacervate systems is intriguing and suggests that additional factors may be critical for understanding the dynamics of these systems. For instance, several reports have described a reduction in the rate of chain as a result of pH changes designed to decrease the charge density of one or more of the polyelectrolytes (Fig. 7b) [75,103]. Teka et al., have speculated that this decrease in chain dynamics is due to an increase in hydrophobic interactions from the uncharged segments of the chain [103]. Additional studies are needed to further elucidate this subtle interplay of interactions.

### 3.2.1. Time–salt superposition

Spruijt et al. proposed a way of overcoming the experimental limitations of a single sample through the use of a time–salt superposition [79,111]. Superposition has long been used as a tool in rheology where an experimental variable such as temperature or strain rate is used as a means for accelerating activated processes. Thus, while a single sample

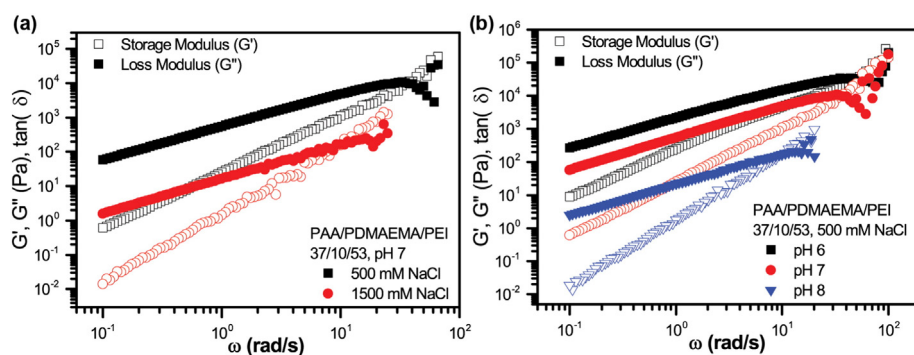


**Fig. 7.** Frequency sweep data for ternary coacervates composed of the polyanion PAA in complex with the polycations PDMAEMA and PEI in a molar ratio of 37/10/53 (a) as a function of NaCl concentration at pH 7, and (b) at 500 mM NaCl, as a function of pH. The shift in the crossover point to lower frequency is indicative of longer relaxation times. Figures adapted with permission from Ref. [75] (Priftis et al., *Macromolecules*, (2014), 47, 3076–3085). Copyright 2014 American Chemical Society.

might only allow for exploration of material properties over a small range of timescales, superposition allows for the combination of multiple datasets to explore a much wider range of frequency space. Similar to time–temperature superposition methods used for other soft materials, the addition of salt provides a means for accelerating an activated process (e.g., rearrangement of electrostatic linkages). Consequently, it is possible to convert a series of frequency sweeps for samples of complex coacervates prepared at different salt conditions (Fig. 9a), which may only span a few decades of frequency space, into a master curve that spans more than eight decades of frequency space (Fig. 9b). This larger presentation of data clearly shows the characteristics of the terminal region, as well as the crossover point and a rubbery plateau. Ultimately, the limitations of the accessible dynamic range for this type of superposition are dictated by artifacts related to the inertia of the instrument itself, edge failure, the potential for secondary flows, etc. [117], coupled with the minimum achievable salt concentration to form coacervates, and the critical salt concentration above which coacervation no longer occurs.

The rescaling was performed using salt concentration-dependent shift factors in both frequency and modulus space. This scaling can be performed using an arbitrary choice of reference. However, in the work presented by Spruijt et al. [79,111], as well as in subsequent reports by other groups [71], the crossover point between the two moduli was chosen as the reference. Inspection of the temporal shift factors (Fig. 9c) suggests an exponential-like dependence of the shift factor on salt concentration, over a wide range of polymer molecular weights. Mechanistically, time–salt superposition assumes that the addition of

salt allows for the acceleration of an activated process. For the proposed model of “sticky” Rouse dynamics, where friction arises from electrostatic interactions between polyelectrolyte chains, the average lifetime for an ionic bond can be described as using an Arrhenius type expression for the activation energy for the interaction. Thus, the activation energy for these interactions can be described as an exponential, which is a function of salt. Only a weak dependence was observed for the modulus shift factor as a function of salt concentration (Fig. 9d). This model provides a powerful means for coupling mechanical measurements to thermodynamic quantities that can be accessed directly by other experimental and theoretical approaches.

### 3.2.2. Time–pH superposition

Tekaat et al., recently coupled the ideas of time–salt superposition with a new demonstration of time–pH superposition (Fig. 10). This principle implied that the changes in polyelectrolyte charge density resulting from changing pH only influence the timescale of the relaxation dynamics, rather than altering the mechanism of their interaction. This work utilized complex coacervates composed of PAA, a weak polyanion, and PDADMAC, a strong polycation, in the presence of KCl [103]. Thus, at high pH both of the polymers will be fully charged, while the charge density of the polyanion will decrease at more acidic pH values. Calculated shift factors showed a clear pH dependence that plateaus at pH  $\approx$  7, where the PAA becomes fully charged (Fig. 10c). The pH dependence of the shift factors can be further extended to the physical state of the polyelectrolyte based on the degree of dissociation ( $\alpha$ ) of the PAA (Fig. 10d). This deconvolution highlights the interplay between polyelectrolyte charge density, pH, and salt concentration. Examination of the data and the shift factors reveals a decrease in chain dynamics with decreasing charge density that may be due to increasing friction from the uncharged, hydrophobic sections of the PAA. The ability to directly relate changes in relaxation behavior to the degree of dissociation of a polyelectrolyte has significant potential to help elucidate apparent disparities in the reported literature between different material systems.

### 3.3. Relaxation time spectra

The relaxation behavior of a material can be expressed equivalently in terms of the relaxation modulus  $G(t)$  as a function of the strain rate history for  $-\infty < t' < t$ , and the relaxation time spectrum  $H(\tau)$  for all relaxation modes  $\tau \leq \tau_{\max}$  [79,123].

$$\sigma(t) = \int_{-\infty}^t G(t-t') \frac{d\gamma}{dt'} dt' \quad (4)$$

$$G(t) = \int_0^{\tau_{\max}} \frac{d\tau}{t} H(\tau) e^{-\tau/t} \quad (5)$$

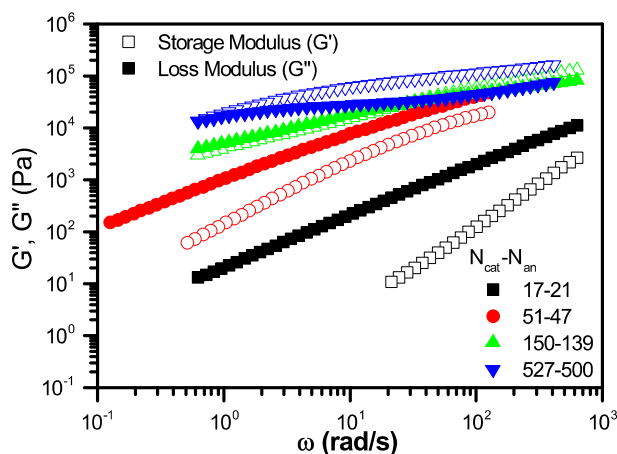


**Fig. 8.** Frequency sweep data for stoichiometric (1:1) PDMAEMA/PAA coacervates with increasing polymer chain length, formed in 0.5 M KCl, pH 6.5. The shift in the crossover point to lower frequency with increasing polymer chain length is indicative of an increase in the relaxation timescale for the system. Figure adapted with permission from Ref. [79] (Spruijt et al., *Macromolecules*, (2013), 46, 1633–1641). Copyright 2013 American Chemical Society.

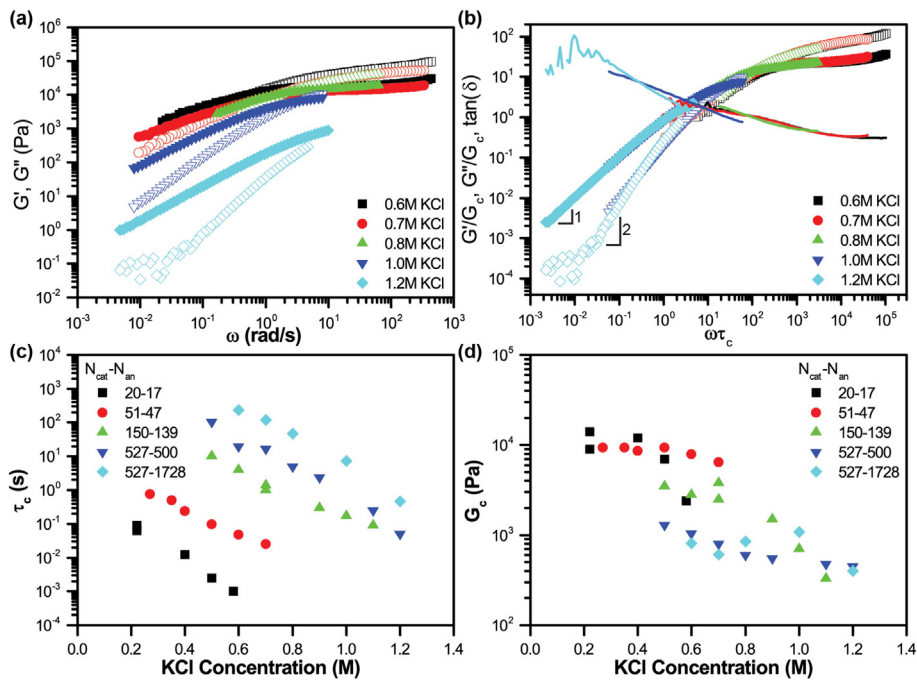


**Fig. 9.** (a) Frequency sweep data for stoichiometric PDMAEMA/PAA coacervates prepared in KCl solutions at pH 6.5 with an average degree of polymerization of  $N = 527$  for PDMAEMA and  $N = 1728$  for PAA. The storage modulus  $G'$  is shown in open symbols, the loss modulus  $G''$  is shown in closed symbols. (b) A rescaled time–salt superposition of the data from (a) where the frequencies have been rescaled using a salt-dependent shift factor  $\tau_c$  shown in (c), and the storage (open) and loss moduli (closed) have been rescaled using a salt-dependent shift factor  $G_c$  shown in (d). The continuity of the  $\tan(\delta)$  plot (line) demonstrates the quality of the superposition. The crossover between  $G'$  and  $G''$  was taken as the reference condition to define  $\omega\tau_c = 1$  and  $G'/G_c = 1$ .

Figures adapted with permission from Ref. [79] (Spruijt et al., *Macromolecules*, (2013), 46, 1633–1641). Copyright 2013 American Chemical Society.

These material functions can be obtained both from conversion of frequency sweep data, and directly from a step-strain experiment. In a step-strain experiment, an instantaneous shear strain is applied to the sample and the resulting stress is allowed to relax over time while the strain is held constant. Thus, the step-strain experiment is able to

probe and identify the entire range of dynamic timescales for a given material, including the terminal relaxation time (i.e.,  $\tau_3$  in Fig. 12). For the system of PDMAEMA/PAA utilized by Spruijt et al., a continuous decrease of the relaxation modulus was observed for all coacervate samples, regardless of salt concentration or polymer chain length

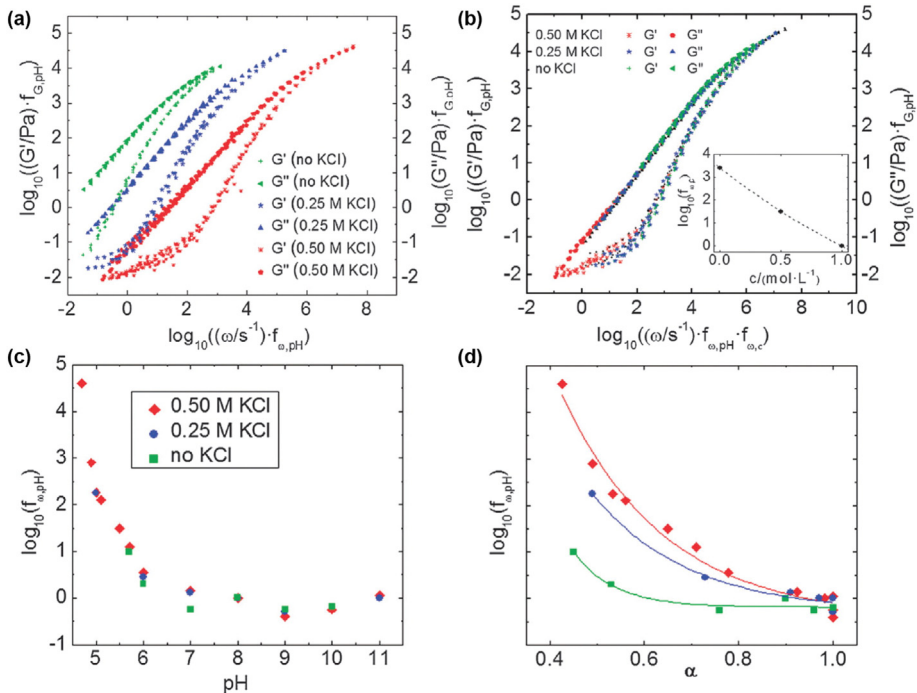


**Fig. 10.** (a) Master curves resulting from the time–pH superposition of frequency sweep data for stoichiometric PDADMAC/PAA coacervates prepared at various KCl and pH conditions. (b) A super-master curve combining the time–pH superposition from (a) with a subsequent time–salt superposition. The inset shows the scaling factors used for this procedure. Shift factors for the superposition shown in (a) as a function of (c) pH and (d) the dissociation constant ( $\alpha$ ) for PAA. Lines are provided as a guide to the eye. Figures adapted from Ref. [79] with permission from the PCCP Owner Societies.

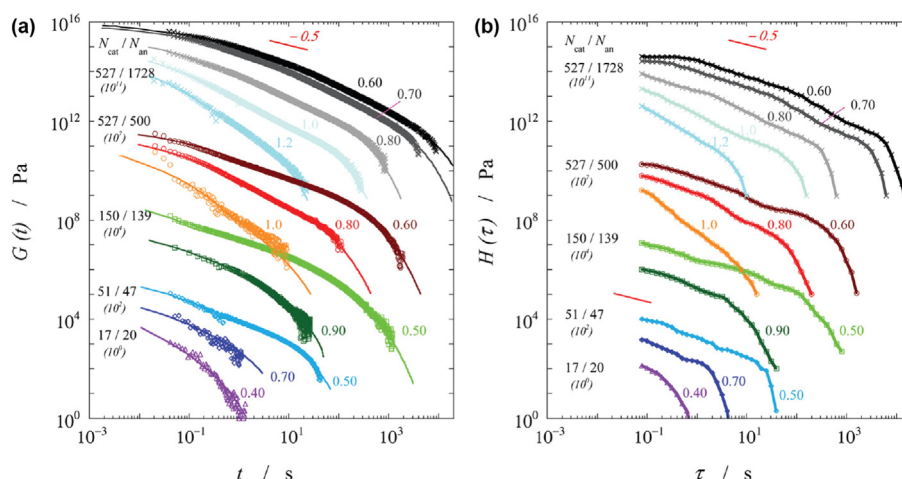


**Fig. 11.** (a) Stress relaxation modulus for stoichiometric PDMAEMA/PAA coacervates prepared in different concentration KCl solutions (labels on the right of the curves) at pH 6.5 and for different polymer chain lengths (labels on the left of the curves, i.e.,  $N_{\text{cat}}/N_{\text{an}}$  for the polycation and polyanion, respectively). A step strain of 10–20% was applied. (b) Relaxation time spectra for the same samples as in (a). All curves are shifted vertically for clarity using the shift factor shown in parentheses at the left of the curves. Figures adapted with permission from Ref. [79] (Spruijt et al., *Macromolecules*, (2013), 46, 1633–1641). Copyright 2013 American Chemical Society.

(Fig. 11a) [79]. At short times (tens of milliseconds), a region of constant slope, of the order  $-0.5$  to  $-0.7$  is observed – a characteristic for the Rouse or Zimm dynamics referenced previously. Thus, at short length scales, Zimm relaxation modes such as hydrodynamic interactions are expected to dominate the polymer dynamics, while at longer length scales Rouse modes will be more dominant.

Closer examination of the data in Fig. 11 indicates that, for these experiments, neither salt concentration nor chain length has a significant effect on the shape of the relaxation spectra, although relaxation processes are observed from the millisecond to the terminal relaxation time. The terminal relaxation time was seen to increase with increasing polymer chain length and decreasing salt concentration. Thus, it is possible to perform a time–salt superposition of the relaxation spectra (Fig. 12) [79]. Just as time–salt superposition allowed for comparison of dynamics in frequency space, here, the technique allows for a more direct comparison of relaxation phenomena occurring within the coacervate material in the presence of different salt concentrations. In the various relaxation spectra shown in Figs. 11 and 12, three different

regimes are present. The terminal relaxation time is indicated by  $\tau_3$ . At intermediate timescales ( $\tau_2 < t < \tau_3$ ), Rouse-like stress relaxation is observed, with a characteristic slope of  $-0.5$ . At short timescales ( $\tau_1 < t < \tau_2$ ), a plateau-like behavior is observed, followed by an upturn ( $t < \tau_1$ ) for the longest polymer chains. The onset of this plateau region ( $\tau_2$ ) can be thought of as the elementary lifetime of a single “sticky” unit, which for a coacervate material would be an ionic bond. At 0.6 M KCl, this lifetime is approximated at 200 ms, which is in agreement with previously reported single-molecule force spectroscopy experiments [181].

## 4. Other applications of dynamics

### 4.1. Encapsulation and release

In addition to characterization of the properties of the base material, rheology has been used to understand the impact that a guest molecule has on the structure of a complex coacervate. Tiwari et al., examined both the encapsulation and release of salbutamol sulfate, a bronchodilator used in the treatment of asthma and other chronic airway diseases, from coacervates formed from a pair of protein molecules, gelatin-A and gelatin-B [141]. Linear viscoelastic characterization showed that drug encapsulation caused a significant decrease in the storage modulus ( $G'$ ), suggesting that the coacervate matrix was disturbed and weakened by the presence of the drug, and a slight increase in the loss modulus ( $G''$ ), suggesting a commensurate fluidization of the material. Such changes in material properties can be critical for modeling of release processes for more advanced therapeutics.

### 4.2. Gelation

Gelation is a phenomenon that connects with complex coacervation in several ways. Firstly, the application of temperature to many of the materials used in coacervation, and proteins in particular, can lead to a gelation phenomenon. In protein-based systems such as those involving gelatin, this type of gel formation is often the result of temperature or pH-induced protein denaturation [137,182]. Solid-to-liquid transitions such as gelation can be observed from a plot of  $\tan(\delta)$  versus frequency. Liquid-like samples will display a negative slope of  $\tan(\delta)$  versus frequency, solid, or gel-like samples will show a positive slope, and the gel point is characterized by zero slope.

Alternatively, one can plot the complex viscosity as a function of frequency and perform a Winter–Chambon model power-law analysis (Fig. 13a) [178,183]. In the Winter–Chambon model, the complex viscosity of a critical gel scales as  $\eta^* = S\omega^{n-1}$ , where  $S$  is the elastic

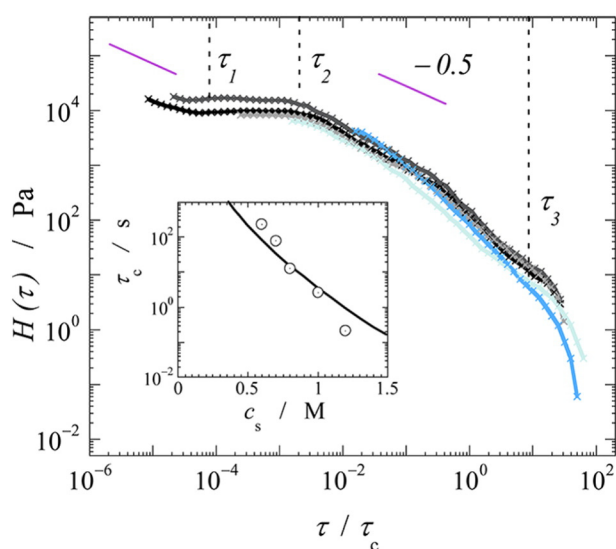


**Fig. 12.** Rescaled relaxation time spectra for stoichiometric PDMAEMA/PAA coacervates with polymer chain length  $N_{\text{cat}}/N_{\text{an}} = 527/1728$ , prepared at different concentration KCl solutions, pH 6.5. The inset shows the scaling factors as a function of salt concentration. Figure adapted with permission from Ref. [79] (Spruijt et al., *Macromolecules*, (2013), 46, 1633–1641). Copyright 2013 American Chemical Society.

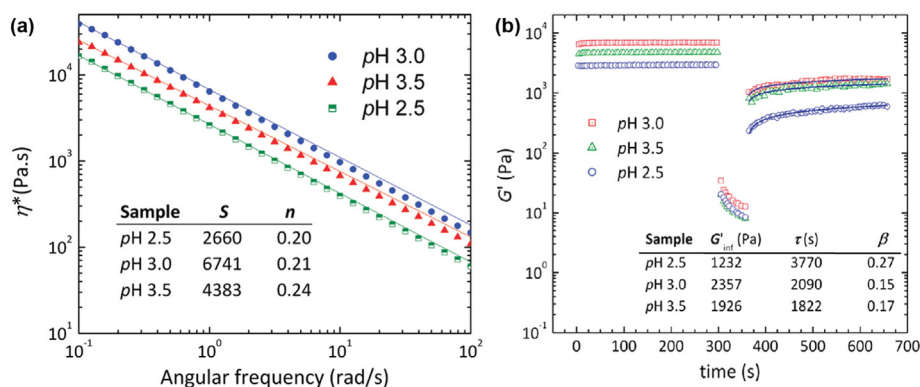


**Fig. 13.** (a) Complex viscosity,  $\eta^*$  vs angular frequency for fish gelatin/sodium montmorillonite (clay nanoplatelets) coacervates prepared at different pH conditions. The solid lines are  $\eta^* = S\omega^n - 1$  (Winter-Chambon model) fitting to the data points. The inset table lists the model parameters. (b) Structural recovery behavior as a function of time, assessed by monitoring  $G'$  after the application of a 100% oscillatory shear strain. The solid lines in regime III are fitting of  $G' = G'_{\infty}(1 - \exp(-t/\tau)^{\beta})$  to the data points. The inset table lists the fitting parameters.

Figures adapted with permission from Ref. [178] (Qazvini et al., *Biomacromolecules*, (2012), 13, 2136–2147). Copyright 2012 American Chemical Society.

strength of the material, and the exponent  $n$  is indicative of the nature of the crosslinking in the material. The measured exponent value reported for a coacervate system composed of fish gelatin/sodium montmorillonite (clay nanoplatelets) was on the order of 0.20–0.24, in the range characteristic of a gel-like system, although with significantly higher water content than a more classical gel [178].

#### 4.3. Self-healing and structural recovery

Another interesting material property conferred by the non-covalent nature of the molecular interactions defining complex coacervates is the potential for self-healing and structural recovery after complete network disruption [174,178]. This can be assayed by the application of a large strain (i.e., 100% oscillatory shear strain, well beyond the linear range for the material) to break the sample, followed by continuous measurements back in the linear strain regime to track the ability of the material to recover its original elasticity, and the requisite timescale to do so. An example of this type of experiment is given for a fish gelatin/sodium montmorillonite coacervate system in Fig. 13b [178]. From an initially high value for the equilibrium storage modulus ( $G'$ ), the application of a high strain decreases the modulus of the material, breaking the internal elastic network of electrostatic interactions and converting it into a liquid-like material. Five minutes after the application of this high strain, the sample was able to recover 20–30% of its original modulus – a process that could be modeled by an exponential function. Furthermore, the timescale for strain recovery was found to be an inverse function of pH, or the number of available electrostatic crosslinks in the system, with more weakly crosslinked systems (i.e., lower pH samples) showing lower fragility and faster recovery. Interestingly, examination of the effects network disruption in the example by Qazvini et al., suggested that the liquid-like behavior was not the result of free-flowing individual nanoplatelets, but rather the result of domain fracturing. Upon removal of strain, these domains are then able to quickly recover the percolated elastic behavior of a network to give a solid-like response, followed by a slower rearrangement of the gelatin network. This self-healing capability suggests that these types of materials could be easily processed as low viscosity materials, for example as thin films or injectables, followed by a recovery time to allow for the formation of an elastic gel.

#### 4.4. Hierarchically-structured coacervate-based materials

While the bulk of the discussion in this review has focused on the viscoelastic characterization of macrophase separated coacervate materials, a wide variety of hierarchically-structured coacervate-based materials have also been reported [63,68,69,101,102,107,184–189]. In these

materials, coupling of a polyelectrolyte to a neutral, water-soluble polymer such as poly(ethylene glycol) facilitates the creation of a molecular interface, and drives microphase separation. Diblock copolymer systems have been reported to form micellar and vesicular structures [69,101,102,187,188], while triblock copolymer systems can form flower-like micelles under dilute conditions, and structured, hydrogel-like materials at higher polymer concentrations [63,68,184–186,189].

Krogstad et al., examined the structural and rheological response of a model triblock copolymer coacervate system composed of guanadinium and sulfonate functionalized poly[(allyl glycidyl ether)-*b*-(ethylene oxide)-*b*-(allyl glycidyl ether)] (PAGE<sub>31</sub>-PEO<sub>455</sub>-PAGE<sub>31</sub>), ABA triblock copolymers. At low polymer concentrations, X-ray and neutron scattering data demonstrated the presence of a disordered network of nanometer-scale coacervate spheres. With increasing polymer concentration, spheres packed into a body-centered cubic (BCC) array, and ultimately transitioned into a hexagonal network of cylinders (Fig. 14c) [68,186]. Frequency sweep analysis showed an increase in modulus and a shift in the crossover point to lower frequency with increasing polymer concentration (Fig. 14a) up to 25 wt.%, followed by a decrease in these parameters at 30 wt.%. Three regimes of behavior were observed, corresponding with the structural transitions observed in the material. The response of the disordered array of spheres (<15 wt.%) was that of a complex fluid, largely dominated by the loss modulus ( $G''$ ) for most of the frequency range. Between 15 wt.% and 25 wt.%, a large increase in the storage modulus ( $G'$ ) was observed, corresponding to the stiffer nature of the BCC array of coacervate domains. Finally, the decrease in modulus observed above 25 wt.% corresponded to the transformation to a hexagonally packed array of cylinders. The authors proposed that the reduction in modulus was due to the ability of the cylindrical phase to enable liquid-like movement of tethered chains along the cylinder axis.

Equilibration and ordering within the hydrogel materials was further tested using time-sweep experiments, where the evolution of the sample was observed at 1% strain for 2000 s. The sample was then disrupted by 100% strain, and the recovery examined (Fig. 14b) [68,186]. All samples showed a time-dependent stiffening during the initial equilibration period. However, following the application and release of high strain the 10 wt.% and 20 wt.% samples (i.e., disordered spheres and BCC spheres) showed an increase in modulus, while the 30% sample (hexagonal cylinders) suffered a decrease in modulus. This decrease in modulus was attributed to the alignment of cylinders parallel to the direction of applied force. These studies demonstrated the convolution of coacervate phase behavior with the complexity of hierarchical ordering within a material. Further study of such materials is needed, along with continued exploration of the available structural motifs.

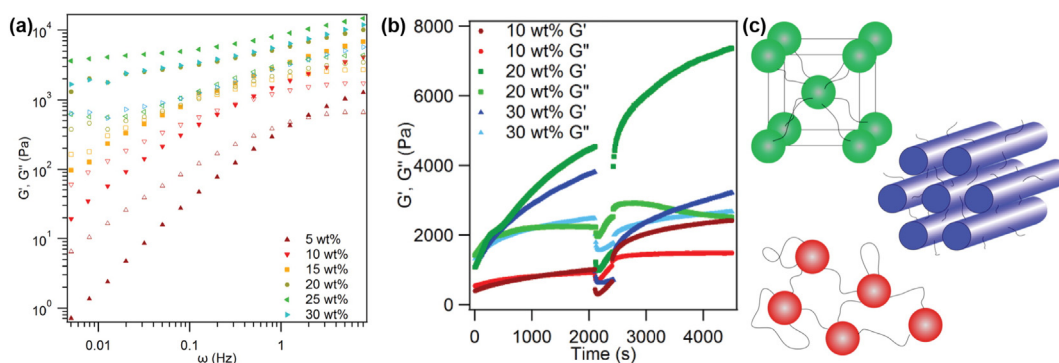


**Fig. 14.** Rheological characterization of hierarchically structured coacervate-based hydrogels formed from the complexation of guanadinium and sulfonate functionalized PAGE<sub>31</sub>-PEO<sub>455</sub>-PAGE<sub>31</sub> ABA triblock copolymers. (a) Frequency sweep data at varying polymer concentrations. The  $G'$  data are shown as solid symbols whereas the  $G''$  data have open symbols. (b) Dynamic mechanical spectra showing the effects of high strain on the ordering of the triblock copolymer gels. After 2000 s at 1% strain, 100% strain was used to break down the gels for 5000 s. After switching back to 1% strain, the 10 wt.% (disordered arrangement of spheres) showed an increase in  $G'$  while the 20 wt.% (BCC spheres) showed a slight increase and the 30 wt.% (hexagonal cylinders) showed a decrease in  $G'$ . (c) Schematic depictions of the BCC spheres, hexagonal cylinders, and disordered arrangement of connected spheres, color-coded and arranged to match the data in (b). Figures adapted from Ref. [186], with permission.

#### 4.5. Linear viscoelasticity in vitro and in vivo

While traditional rheological and linear viscoelasticity experiments are extremely powerful, they can suffer from the need to generate sufficient sample. This limitation is particularly challenging for the study of biologically-relevant liquid–liquid phase separation phenomena inside cells. For these materials, which are often termed “membraneless organelles,” the quantity of material, as well as the need to extract such cellular granules from their native environment prevent the application of the types of large-scale SAOS measurements described thus far. However, Elbaum-Garfinkle et al., recently reported the use of microrheology techniques to coacervate-like materials formed as a result of the self-interaction of LAF-1, a DDX3 RNA helicase found in the P granules of *Caenorhabditis elegans* [190]. Here, confocal fluorescence microscopy was used in conjunction with particle tracking methodologies to measure the viscosity of coacervate-like droplets of LAF-1 both with and without RNA. A more detailed treatment of this type of microrheological characterization is beyond the scope of the current work. However, adoption of these types of techniques has the potential to enable the analysis of a vast array of coacervate-based materials that would otherwise be inaccessible to larger-scale rheological measurements.

#### 5. A survey of materials rheology in complex coacervates

The goal of this review is to provide an introduction to the use of linear viscoelastic measurements for the characterization of complex coacervate-based materials. During the course of this presentation, we have focused on only a few materials systems, so as to facilitate the clear presentation of concepts and trends. However, such a limited presentation is by no means representative of the scope of rheological work that has been reported to date. In the following tables, we have attempted to summarize the various cationic (Table 1) and anionic (Table 2) materials used in the formation of complex coacervate-based materials that have been subjected to viscoelastic characterization.

#### 6. Perspective and future vision

The ability to link thermodynamic knowledge of complex coacervate phase behavior with data describing the dynamics of a material, such as the characteristic timescales for molecular motion, is a critical next step towards the development of a fundamental and predictive understanding of this self-assembly phenomenon. The breadth of work reported thus far has provided tantalizing glimpses of the potential for coacervate-based materials. Moving forward, there is a pressing

**Table 1**

Summary of cationic macro-ions examined via rheological characterization of complex coacervates.

Name	Strong/Weak	Type	References
$\alpha$ -Lactalbumin	Weak	Protein	[174,179]
$\beta$ -Lactoglobulin	Weak	Protein	[174,179,180]
Bovine serum albumin (BSA)	Weak	Protein	[8,87,138,179]
Chitosan	Weak	Polysaccharide	[130,173]
Gelatin	Weak	Protein	[178]
Gelatin A	Weak	Protein	[9,137,141,173,177]
Gelatin B	Weak	Protein	[126,141,175,182]
Jeffamine	Weak	Polymer	[192]
Lactoferrin	Weak	Protein	[95]
LAF-1	Weak	Protein	[190]
mfp1	Weak	Protein	[193]
mfp151	Weak	Protein	[193]
O-carboxymethyl chitosan	Weak	Polysaccharide	[194]
Poly(allylamine hydrochloride)	Weak	Polymer	[61,75]
Poly(diallyldimethylammonium chloride)	Strong	Polymer	[75,87,103,112,157,172,195]
Poly(ether) amine (Jeffamine)	Weak	Polymer	[192]
Poly(ethyleneimine)	Weak	Polymer	[71,75]
Poly(N,N-dimethylaminoethyl methacrylate)	Weak	Polymer	[79,111]
Wheat Protein	Weak	Protein	[9]
Whey Protein Isolate	Weak	Protein	[174,179]

**Table 2**  
Summary of anionic macro-ions examined via rheological characterization of complex coacervates.

Name	Strong/weak	Type	References
Agar	Strong	Polysaccharide	[126,179]
Alginate	Weak	Polysaccharide	[192,196]
$\beta$ -Lactoglobulin	Weak	Protein	[95,180,182]
DNA	Strong	Nucleic acid	[137,177]
Gelatin	Weak	Protein	[124]
Gelatin A	Weak	Protein	[141,173]
Gelatin B	Weak	Protein	[141,175,182]
Gum Arabic	Weak	Polysaccharide	[130,174,194]
Hyaluronic acid	Weak	Polysaccharide	[193]
$\kappa$ -Carrageenan	Strong	Polysaccharide	[8]
Pectin	Weak	Polysaccharide	[138,180]
Poly(acrylic acid)	Weak	Polymer	[75,79,103,111]
Poly(aspartic acid)	Weak	Polypeptide	[71,193]
Poly(glutamic acid)	Weak	Polypeptide	[71]
Poly(styrene sulfonate)	Strong	Polymer	[124,157,195]
Polyphosphate	Strong	Polymer	[171]
Pyrophosphate	Strong	Small molecule	[61]
RNA	Strong	Nucleic acid	[190]
Sodium dodecylsulfate	Strong	Surfactant	[112,172]
Sodium montmorillonite	Weak	Clay particle	[178]
Soy Protein	Weak	Protein	[9,196]
Tripolyphosphate	Strong	Small molecule	[61]
Xanthan gum	Weak	Polysaccharide	[196]

need for a systematic evaluation of the different variables associated with coacervate formation, particularly those related to the structure and chemistry of the materials themselves. For instance, what effect does changing the identity of the charged group have on material properties? What impact does side-chain length have on polyelectrolyte-based coacervation? What is the effect of branching or other architectures? How do sequences of chemistry or localized patches of charge affect not only self-assembly, but the resultant dynamic response of the material?

Moving beyond knowledge of composition and dynamics, further levels of understanding require incorporation of knowledge regarding the molecular structure of coacervate-based materials, and the development of more detailed theories and models. Hybrid techniques, such as simultaneous small-angle X-ray or small-angle neutron scattering, coupled with rheology (rheo-SAXS/SANS) [124], rheo-optics [117,191], calorimetry, and/or other methods have tremendous potential to further expand our understanding of this class of materials. Subsequent interpretation of the resulting data will require the further development and validation of theoretical predictions to couple observation with molecular models. For instance, the systematic linear viscoelastic analysis of polymer chemistry effects on complex coacervation would enable further testing of the “sticky” Rouse model proposed by Spruijt et al. [79,111]. Such efforts could also be coupled with advancements in the modeling of coacervation in general. It is important to note, that the vast majority of experimental and theoretical efforts have focused on understanding SAOS data because of the strong theoretical background of such measurements. However, from an applications perspective, most processing operations subject materials to deformations that are well beyond the limits of linear viscoelasticity. Extension of theoretical treatments of polymer behavior into the non-linear large-angle oscillatory shear (LAOS) regime, has tremendous potential to elucidate critical mechanisms related to the large-scale disruption and rearrangements of polymer networks. The application of such non-linear techniques to the characterization of complex coacervate-based materials is an open challenge for the future.

## Acknowledgements

We would like to thank Dr. Evan Spruijt, Dr. Dimitrios Priftis, Dr. Daniel Krogstad, and Prof. Joseph Schlenoff for their generosity in sharing experimental data. We would also like to thank Dr. Samanvaya

Srivastava, Prof. Charles E. Sing, and Prof. Jessica D. Schiffman for helpful discussions.

## References

- [1] van der Gucht J, Spruijt E, Lemmers M, Cohen Stuart MA. Polyelectrolyte complexes: bulk phases and colloidal systems. *J Colloid Interface Sci* 2011;361:407–22. <http://dx.doi.org/10.1016/j.jcis.2011.05.080>.
- [2] de Kruijff CG, Weinbreck F, de Vries R. Complex coacervation of proteins and anionic polysaccharides. *Curr Opin Colloid Interface Sci* 2004;9:340–9. <http://dx.doi.org/10.1016/j.cocis.2004.09.006>.
- [3] Priftis D, Laugel N, Tirrell M. Thermodynamic characterization of polypeptide complex coacervation. *Langmuir* 2012;28:15947–57. <http://dx.doi.org/10.1021/la302729r>.
- [4] Fu J, Schlenoff JB. Driving forces for oppositely charged polyion association in aqueous solutions: enthalpic, entropic, but not electrostatic. *J Am Chem Soc* 2016;138:980–90. <http://dx.doi.org/10.1021/jacs.5b11878>.
- [5] Madene A, Jacquot M, Scher J, Desobry S. Flavour encapsulation and controlled release – a review. *Int J Food Sci Technol* 2006;41:1–21. <http://dx.doi.org/10.1111/j.1365-2621.2005.00980.x>.
- [6] Augustin MA, Hemar Y. Nano- and micro-structured assemblies for encapsulation of food ingredients. *Chem Soc Rev* 2009;38:902–12.
- [7] Tavares GM, Croguennec T, Hamon P, Carvalho AF, Bouhallab S. Selective coacervation between lactoferrin and the two isoforms of  $\beta$ -lactoglobulin. *Food Hydrocolloids* 2015;48:238–47. <http://dx.doi.org/10.1016/j.foodhyd.2015.02.027>.
- [8] Chai C, Lee J, Huang Q. The effect of ionic strength on the rheology of pH-induced bovine serum albumin/ $\kappa$ -carrageenan coacervates. *LWT-Food Sci Technol* 2014;59:356–60.
- [9] Firoozmand H, Rousseau D. Microstructure and rheology design in protein–protein–polysaccharide composites. *Food Hydrocolloids* 2015;50:84–93. <http://dx.doi.org/10.1016/j.foodhyd.2015.04.003>.
- [10] Davidov-Pardo G, Joye JJ, McClements DJ. Food-grade protein-based nanoparticles and microparticles for bioactive delivery: fabrication, characterization, and utilization. *Advances in Protein Chemistry and Structural Biology*, vol. 98. Elsevier Inc.; 2015. p. 293–325. <http://dx.doi.org/10.1016/bs.apcsb.2014.11.004>.
- [11] Okuro PK, Furtado GF, Sato ACK, Cunha RL. Science direct structures design for protection and vehiculation of bioactives. *Curr Opin Food Sci* 2015;5:67–75. <http://dx.doi.org/10.1016/j.cofs.2015.09.003>.
- [12] Wu B-C, Degner B, DJ MC. Soft matter strategies for controlling food texture: formation of hydrogel particles by biopolymer complex coacervation. *J Phys Condens Matter* 2014;26:464104. <http://dx.doi.org/10.1088/0953-8984/26/46/464104>.
- [13] Gibson SM. Heat-stable protein microparticles and no-shear process for producing same; 1998.
- [14] Seweryn A, Wasilewski T, Bujak T. Effect of salt on the manufacturing and properties of hand dishwashing liquids in the coacervate form. *Ind Eng Chem Res* 2016;55:1134–41. <http://dx.doi.org/10.1021/acs.iecr.5b04048>.
- [15] Kalantar TH, Tucker CJ, Zalusky AS, Boomgaard TA, Wilson BE, Ladika M, et al. High throughput workflow for coacervate formation and characterization in shampoo systems. *J Cosmet Sci* 2007;58:375–83.
- [16] Pergushov DV, Müller AHE, Schacher FH. Micellar interpolyelectrolyte complexes. *Chem Soc Rev* 2012;41:6888–901. <http://dx.doi.org/10.1039/c2cs35135h>.
- [17] Kayitmazer AB, Seeman D, Minsky BB, Dubin PL, Xu Y. Protein–polyelectrolyte interactions. *Soft Matter* 2013;9:2553–83. <http://dx.doi.org/10.1039/c2sm27002a>.
- [18] Jewell CM, Lynn DM. Multilayered polyelectrolyte assemblies as platforms for the delivery of DNA and other nucleic acid-based therapeutics. *Adv Drug Deliv Rev* 2008;60:979–99. <http://dx.doi.org/10.1016/j.addr.2008.02.010>.
- [19] Jewell CM, Lynn DM. Surface-mediated delivery of DNA: cationic polymers take charge. *Curr Opin Colloid Interface Sci* 2008;13:395–402. <http://dx.doi.org/10.1016/j.cocis.2008.03.005>.
- [20] Chu H, Johnson NRY, Mason NS, Wang Y. A [polycation:heparin] complex releases growth factors with enhanced bioactivity. *J Control Release* 2011;150:157–63. <http://dx.doi.org/10.1016/j.jconrel.2010.11.025>.
- [21] Chu H, Gao J, Chen C-W, Huard J, Wang Y. Injectable fibroblast growth factor-2 coacervate for persistent angiogenesis. *Proc Natl Acad Sci U S A* 2011;108:13444–9. <http://dx.doi.org/10.1073/pnas.1110121108>.
- [22] Pittella F, Kataoka K. Polymeric micelles for siRNA delivery. In: Howard KA, editor. *Advances in delivery science and technology*. US: Springer; 2012. p. 161–84. [http://dx.doi.org/10.1007/978-1-4614-4744-3\\_8](http://dx.doi.org/10.1007/978-1-4614-4744-3_8).
- [23] Zern BJ, Chu H, Wang Y. Control growth factor release using a self-assembled [polycation:heparin] complex. *PLoS One* 2010;5, e11017. <http://dx.doi.org/10.1371/journal.pone.0011017>.
- [24] Jewell CM, Zhang J, Fredin NJ, Lynn DM. Multilayered polyelectrolyte films promote the direct and localized delivery of DNA to cells. *J Control Release* 2005;106:214–23. <http://dx.doi.org/10.1016/j.jconrel.2005.04.014>.
- [25] Jewell CM, Zhang J, Fredin NJ, Wolff MR, Hacker TA, Lynn DM. Release of plasmid DNA from intravascular stents coated with ultrathin multilayered polyelectrolyte films. *Biomacromolecules* 2006;7:2483–91. <http://dx.doi.org/10.1021/bm0604808>.
- [26] Dimitrova M, Arntz Y, Lavalle P, Meyer F, Wolf M, Schuster C, et al. Adenoviral gene delivery from multilayered polyelectrolyte architectures. *Adv Funct Mater* 2007;17:233–45. <http://dx.doi.org/10.1002/adfm.200600155>.
- [27] Flessner RM, Jewell CM, Anderson DG, Lynn DM. Degradable polyelectrolyte multilayers that promote the release of siRNA. *Langmuir* 2011;27:7868–76. <http://dx.doi.org/10.1021/la200815t>.
- [28] Bechler SL, Lynn DM. Characterization of degradable polyelectrolyte multilayers fabricated using DNA and a fluorescently-labeled poly( $\beta$ -amino ester): shedding light on the role of the cationic polymer in promoting surface-mediated gene delivery. *Biomacromolecules* 2012;13:542–52. <http://dx.doi.org/10.1021/bm2016338>.
- [29] Ghobadi AF, Letteri R, Parelkar SS, Zhao Y, Chan-Seng D, Emrick T, et al. Dispersing zwitterions into comb polymers for nonviral transfection: experiments and molecular simulation. *Biomacromolecules* 2016;17:546–57. <http://dx.doi.org/10.1021/acs.biomac.5b01462>.

- [30] Jiang Y, Lu H, Chen F, Callari M, Pourgholami M, Morris DL, et al. PEGylated albumin-based polyion complex micelles for protein delivery. *Biomacromolecules* 2016;17:808–17. <http://dx.doi.org/10.1021/acs.biomac.5b01537>.
- [31] Johnson NR, Kruger M, Goetsch KP, Zilla P, Bezuidenhout D, Wang Y, et al. Coacervate delivery of growth factors combined with a degradable hydrogel preserves heart function after myocardial infarction. *ACS Biomater Sci Eng* 2015;1:753–9. <http://dx.doi.org/10.1021/acsbomaterials.5b00077>.
- [32] Johnson NR, Wang Y. Coacervate delivery systems for proteins and small molecule drugs. *Expert Opin Drug Discovery* 2014;11:1829–32. <http://dx.doi.org/10.1517/17425247.2014.941355>.
- [33] Johnson NR, Wang Y. Controlled delivery of heparin-binding EGF-like growth factor yields fast and comprehensive wound healing. *J Control Release* 2013;166:124–9. <http://dx.doi.org/10.1016/j.jconrel.2012.11.004>.
- [34] Johnson NR, Ambe T, Wang Y. Lysine-based polycation:heparin coacervate for controlled protein delivery. *Acta Biomater* 2014;10:40–6. <http://dx.doi.org/10.1016/j.actbio.2013.09.012>.
- [35] Kabanov AV, Vinogradov SV, Suzdaltseva YG, Alakhov VY. Water-soluble block polycations as carriers for oligonucleotide delivery. *Bioconjug Chem* 1995;6:639–43. <http://dx.doi.org/10.1021/bc00036a001>.
- [36] Koppolu BP, Smith SG, Ravindranathan S, Jayanthi S, Kumar TKS, Zaharoff DA. Controlling chitosan-based encapsulation for protein and vaccine delivery. *Biomaterials* 2014;35:4382–9. <http://dx.doi.org/10.1016/j.biomaterials.2014.01.078>.
- [37] Kuo C-H, Leon L, Chung EJ, Huang R-T, Sontag TJ, Reardon CA, et al. Inhibition of atherosclerosis-promoting microRNAs via targeted polyelectrolyte complex micelles. *J Mater Chem B* 2014;2:8142–53. <http://dx.doi.org/10.1039/C4TB00977K>.
- [38] Leong K, Mao H, Truong-Le V, Roy K, Walsh S, August J. DNA-polycation nanospheres as non-viral gene delivery vehicles. *J Control Release* 1998;53:183–93.
- [39] Momeni A, Valliant EM, Brennan-Pierce EP, Shankar JJS, Abraham R, Colp P, et al. Developing an in situ forming polyphosphate coacervate as a new liquid embolic agent: from experimental design to pilot animal study. *Acta Biomater* 2016;32:286–97. <http://dx.doi.org/10.1016/j.actbio.2015.12.012>.
- [40] Ozbas-Turan S, Aral C, Kabasakal L, Keyer-Uysal M, Akbuga J. Co-encapsulation of two plasmids in chitosan microspheres as a non-viral gene delivery vehicle. *J Pharm Pharm Sci* 2003;6:27–32.
- [41] Rasente RV, Imperiale JC, Lázaro-Martínez JM, Gualco L, Oberkersch R, Sosnik A, et al. Dermatan sulfate/chitosan polyelectrolyte complex with potential application in the treatment and diagnosis of vascular disease. *Carbohydr Polym* 2016;144:362–70. <http://dx.doi.org/10.1016/j.carbpol.2016.02.046>.
- [42] Thomasin C, Hö N-T, Merkle HP, Gander B. Drug microencapsulation by PLA/PLGA coacervation in the light of thermodynamics. 1. Overview and theoretical considerations. *J Pharm Sci* 1998;87:259–68. <http://dx.doi.org/10.1021/js970047r>.
- [43] Truong-Le VL, August JT, Leong KW. Controlled gene delivery by DNA-gelatin nanospheres. *Hum Gene Ther* 1998;9:1709–17.
- [44] Truong-Le VL, Walsh SM, Schweibert E, Mao H-Q, Guggino WB, August JT, et al. Gene transfer by DNA-gelatin nanospheres. *Arch Biochem Biophys* 1999;361:47–56.
- [45] Vehlow D, Schmidt R, Gebert A, Siebert M, Lips K, Müller M. Polyelectrolyte complex based interfacial drug delivery system with controlled loading and improved release performance for bone therapeutics. *Nanomaterials* 2016;6:53. <http://dx.doi.org/10.3390/nano6030053>.
- [46] Tangsangaksakri M, Takemoto H, Naito M, Maeda Y, Sueyoshi D, Kim HJ, et al. siRNA-loaded polyion complex micelle decorated with charge-conversional polymer tuned to undergo stepwise response to intra-tumoral and intra-endosomal pHs for exerting enhanced RNAi efficacy. *Biomacromolecules* 2016;17:246–55. <http://dx.doi.org/10.1021/acs.biomac.5b01334>.
- [47] Siyawamwaya M, Choonara YE, Bijukumar D, Kumar P, Toit Du LC, Pillay V. A review: overview of novel polyelectrolyte complexes as prospective drug bioavailability enhancers. *Int J Polym Mater Polym Biomater* 2015;64:955–68. <http://dx.doi.org/10.1080/00914037.2015.1038816>.
- [48] Wei W, Tan Y, Rodriguez NRM, Yu J, Israelachvili JN, Waite JH. A mussel-derived one component adhesive coacervate. *Acta Biomater* 2014;10:1663–70. <http://dx.doi.org/10.1016/j.actbio.2013.09.007>.
- [49] Maier GP, Rapp MV, Waite JH, Israelachvili JN, Butler A. Adaptive synergy between catechol and lysine promotes wet adhesion by surface salt displacement. *Science* 2015;349:628–32. <http://dx.doi.org/10.1126/science.1250556>.
- [50] Hwang DS, Zeng H, Lu Q, Israelachvili J, Waite JH. Adhesion mechanism in a DOPA-deficient foot protein from green mussels. *Soft Matter* 2012;8:5640–8. <http://dx.doi.org/10.1039/C2SM25173F>.
- [51] Ahn BK, Das S, Linstadt R, Kaufman Y, Martinez-Rodriguez NR, Mirshafian R, et al. High-performance mussel-inspired adhesives of reduced complexity. *Nat Commun* 2015;6:8663. <http://dx.doi.org/10.1038/ncomms9663>.
- [52] Shao H, Weerasekare GM, Stewart RJ. Controlled curing of adhesive complex coacervates with reversible periodate carboxylate complexes. *J Biomed Mater Res, Part B* 2011;97A:46–51. <http://dx.doi.org/10.1002/jbm.b.33026>.
- [53] Lim S, Moon D, Kim HJ, Seo JH, Kang IS, Cha HJ. Interfacial tension of complex coacervated mussel adhesive protein according to the Hofmeister series. *Langmuir* 2014;30:1108–15. <http://dx.doi.org/10.1021/la403680z>.
- [54] Kaur S, Weerasekare GM, Stewart RJ. Multiphase adhesive coacervates inspired by the sandcastle worm. *ACS Appl Mater Interfaces* 2011;3:941–4. <http://dx.doi.org/10.1021/am200082v>.
- [55] Hwang DS, Zeng H, Srivastava A, Krogstad DV, Tirrell M, Israelachvili JN, et al. Viscosity and interfacial properties in a mussel-inspired adhesive coacervate. *Soft Matter* 2010;6:3232–6. <http://dx.doi.org/10.1039/c002632h>.
- [56] Stewart RJ, Wang CS, Shao H. Complex coacervates as a foundation for synthetic underwater adhesives. *Adv Colloid Interface Sci* 2011;167:85–93. <http://dx.doi.org/10.1016/j.cis.2010.10.009>.
- [57] Lim S, Choi YS, Kang DG, Song YH, Cha HJ. The adhesive properties of coacervated recombinant hybrid mussel adhesive proteins. *Biomaterials* 2010;31:3715–22. <http://dx.doi.org/10.1016/j.biomaterials.2010.01.063>.
- [58] Wang W, Xu Y, Li A, Li T, Liu M, Klitzing von R, et al. Zinc induced polyelectrolyte coacervate bioadhesive and its transition to a self-healing hydrogel. *RSC Adv* 2015;5:66871–8. <http://dx.doi.org/10.1039/C5RA11915D>.
- [59] Choi YS, Kang DG, Lim S, Yang YJ, Kim CS, Cha HJ. Recombinant mussel adhesive protein fp-5 (MAP fp-5) as a bulk bioadhesive and surface coating material. *Biofouling* 2011;27:729–37. <http://dx.doi.org/10.1080/08927014.2011.600830>.
- [60] Favi PM, Yi S, Lenaghan SC, Xia L, Zhang M. Inspiration from the natural world: from bio-adhesives to bio-inspired adhesives. *J Adhes Sci Technol* 2012;1–30. <http://dx.doi.org/10.1080/10694243.2012.691809>.
- [61] Lawrence PG, Lapitsky Y. Ionically cross-linked poly(allylamine) as a stimulus-responsive underwater adhesive: ionic strength and pH effects. *Langmuir* 2015;31:1564–74. <http://dx.doi.org/10.1021/la504611x>.
- [62] Wilke P, Helfricht N, Mark A, Papastavrou G, Faivre D, Börner HG. A direct biocombinatorial strategy toward next generation, mussel-glue inspired saltwater adhesives. *J Am Chem Soc* 2014;140902165928009. <http://dx.doi.org/10.1021/ja505413e>.
- [63] Hunt JN, Feldman KE, Lynd NA, Deek J, Campos LM, Spruell JM, et al. Tunable, high modulus hydrogels driven by ionic coacervation. *Adv Mater* 2011;23:2327–31. <http://dx.doi.org/10.1002/adma.201004230>.
- [64] Voets IK, de Keizer A, Cohen Stuart MA. Complex coacervate core micelles. *Adv Colloid Interface Sci* 2009;147–148:300–18. <http://dx.doi.org/10.1016/j.cis.2008.09.012>.
- [65] Eulalio A, Behm-Ansant I, Izaurralde E. P bodies: at the crossroads of post-transcriptional pathways. *Nat Rev Mol Cell Biol* 2007;8:9–22. <http://dx.doi.org/10.1038/nrm2080>.
- [66] Kataoka K, Togawa H, Harada A, Yasugi K, Matsumoto T, Katayose S. Spontaneous formation of polyion complex micelles with narrow distribution from antisense oligonucleotide and cationic block copolymer in physiological saline. *Macromolecules* 1996;29:8556–7.
- [67] Hyman AA, Simons K. Beyond oil and water-phase transitions in cells. *Science* 2012;337:1047–9. <http://dx.doi.org/10.1126/science.1223728>.
- [68] Krogstad DV, Lynd NA, Choi S-H, Spruell JM, Hawker CJ, Kramer EJ, et al. Effects of polymer and salt concentration on the structure and properties of triblock copolymer coacervate hydrogels. *Macromolecules* 2013;46:1512–8. <http://dx.doi.org/10.1021/ma302299r>.
- [69] Harada A, Kataoka K. Chain length recognition: core-shell supramolecular assembly from oppositely charged block copolymers. *Science* 1999;283:65–7.
- [70] Patel A, Lee HO, Jawerth L, Maharana S, Jahnel M, Hein MY, et al. A liquid-to-solid phase transition of the ALS protein FUS accelerated by disease mutation. *Cell* 2015;162:1066–77. <http://dx.doi.org/10.1016/j.cell.2015.07.047>.
- [71] Priftis D, Megley K, Laugel N, Tirrell M. Complex coacervation of poly(ethylene-imine)/ polypeptide aqueous solutions: thermodynamic and rheological characterization. *J Colloid Interface Sci* 2013;398:39–50. <http://dx.doi.org/10.1016/j.jcis.2013.01.055>.
- [72] Priftis D, Farina R, Tirrell M. Interfacial energy of polypeptide complex coacervates measured via capillary adhesion. *Langmuir* 2012;28:8721–9. <http://dx.doi.org/10.1021/la300769d>.
- [73] Priftis D, Tirrell M. Phase behaviour and complex coacervation of aqueous polypeptide solutions. *Soft Matter* 2012;8:9396–405. <http://dx.doi.org/10.1039/c2sm25604e>.
- [74] Priftis D, Leon L, Song Z, Perry SL, Margossian KO, Tropnikova A, et al. Self-assembly of  $\alpha$ -helical polypeptides driven by complex coacervation. *Angew Chem Int Ed* 2015;54:11128–32. <http://dx.doi.org/10.1002/anie.201504861R1>.
- [75] Priftis D, Xia X, Margossian KO, Perry SL, Leon L, Qin J, et al. Ternary, tunable polyelectrolyte complex fluids driven by complex coacervation. *Macromolecules* 2014;47:3076–85.
- [76] Perry SL, Leon L, Hoffmann KO, Kade MJ, Priftis D, Black KA, et al. Chirality-selected phase behaviour in ionic polypeptide complexes. *Nat Commun* 2015;6:6052. <http://dx.doi.org/10.1038/ncomms7052>.
- [77] Perry SL, Li Y, Priftis D, Leon L, Tirrell M. The effect of salt on the complex coacervation of vinyl polyelectrolytes. *Polymers* 2014;6:1756–72. <http://dx.doi.org/10.3390/polym6061756>.
- [78] Spruijt E, Westphal AH, Borst JW, Cohen Stuart MA, van der Gucht J. Binodal compositions of polyelectrolyte complexes. *Macromolecules* 2010;43:6476–84. <http://dx.doi.org/10.1021/ma101031t>.
- [79] Spruijt E, Cohen Stuart MA, van der Gucht J. Linear viscoelasticity of polyelectrolyte complex coacervates. *Macromolecules* 2013;46:1633–41. <http://dx.doi.org/10.1021/ma301730n>.
- [80] Spruijt E, Leermakers FAM, Fokkink R, Schweins R, van Well AA, Cohen Stuart MA, et al. Structure and dynamics of polyelectrolyte complex coacervates studied by scattering of neutrons, X-rays, and light. *Macromolecules* 2013;46:4596–605. <http://dx.doi.org/10.1021/ma400132s>.
- [81] Anema SG, de Kruijff CGK. Coacervates of lysozyme and  $\beta$ -casein. *J Colloid Interface Sci* 2013;398:255–61. <http://dx.doi.org/10.1016/j.jcis.2013.02.013>.
- [82] Anema SG, de Kruijff CGK. Co-acervates of lactoferrin and caseins. *Soft Matter* 2012;8:4471–8. <http://dx.doi.org/10.1039/c2sm00015f>.
- [83] Anema SG, de Kruijff CGK. Complex coacervates of lactotransferrin and  $\beta$ -lactoglobulin. *J Colloid Interface Sci* 2014;430:214–20. <http://dx.doi.org/10.1016/j.jcis.2014.05.036>.
- [84] de Kruijff CGK, Pedersen J, Huppertz T, Anema SG. Coacervates of lactotransferrin and  $\beta$ - or  $\kappa$ -casein: structure determined using SAXS. *Langmuir* 2013;29:10483–90. <http://dx.doi.org/10.1021/la402236f>.
- [85] Yan Y, Kizilay E, Seeman D, Flanagan S, Dubin PL, Bovetto L, et al. Heteroprotein complex coacervation: bovine  $\beta$ -lactoglobulin and lactoferrin. *Langmuir* 2013;29:15614–23. <http://dx.doi.org/10.1021/la4027464>.
- [86] Kayitmazer AB, Strand SP, Tribet C, Jaeger W, Dubin PL. Effect of polyelectrolyte structure on protein-polyelectrolyte coacervates: coacervates of bovine serum albumin with poly(diallyldimethylammonium chloride) versus chitosan. *Biomacromolecules* 2007;8:3568–77. <http://dx.doi.org/10.1021/bm700645t>.
- [87] Kizilay E, Kayitmazer AB, Dubin PL. Complexation and coacervation of polyelectrolytes with oppositely charged colloids. *Adv Colloid Interface Sci* 2011;167:24–37.
- [88] Xia J, Mattison K, Romano V, Dubin PL, Muhoberac BB. Complexation of trypsin and alcohol dehydrogenase with poly(diallyldimethylammonium chloride). *Biopolymers* 1997;41:359–65.
- [89] Cooper CL, Goulding A, Kayitmazer AB, Ulrich S, Stoll S, Turksen S, et al. Effects of polyelectrolyte chain stiffness, charge mobility, and charge sequences on binding to proteins and micelles. *Biomacromolecules* 2006;7:1025–35. <http://dx.doi.org/10.1021/bm050592j>.
- [90] Bohidar H, Dubin PL, Majhi PR, Tribet C, Jaeger W. Effects of protein-polyelectrolyte affinity and polyelectrolyte molecular weight on dynamic properties of bovine serum albumin-poly(diallyldimethylammonium chloride) coacervates. *Biomacromolecules* 2005;6:1573–85. <http://dx.doi.org/10.1021/bm049174p>.

- [91] Wang Y, Kimura K, Huang Q, Dubin PL, Jaeger W. Effects of salt on polyelectrolyte–micelle coacervation. *Macromolecules* 1999;32:7128–34. <http://dx.doi.org/10.1021/ma990972v>.
- [92] Kayitmazer AB, Koksals AF, Iyilik EK. Complex coacervation of hyaluronic acid and chitosan: effects of pH, ionic strength, charge density, chain length and the charge ratio. *Soft Matter* 2015;11:8605–12. <http://dx.doi.org/10.1039/C5SM01829C>.
- [93] Kayitmazer AB, Seyrek E, Dubin PL, Staggemeier BA. Influence of chain stiffness on the interaction of polyelectrolytes with oppositely charged micelles and proteins. *J Phys Chem B* 2003;107:8158–65. <http://dx.doi.org/10.1021/jp034065a>.
- [94] Cooper CL, Dubin PL, Kayitmazer AB, Turksen S. Polyelectrolyte–protein complexes. *Curr Opin Colloid Interface Sci* 2005;10:52–78. <http://dx.doi.org/10.1016/j.cocis.2005.05.007>.
- [95] Kizilay E, Seeman D, Yan Y, Du X, Dubin PL, Donato-Capel L, et al. Structure of bovine  $\beta$ -lactoglobulin–lactoferrin coacervates. *Soft Matter* 2014;10:7262–8. <http://dx.doi.org/10.1039/C4SM01333F>.
- [96] Lindhoud S, de Vries R, Schweins R, Cohen Stuart MA, Norde W. Salt-induced release of lipase from polyelectrolyte complex micelles. *Soft Matter* 2009;5:242–50. <http://dx.doi.org/10.1039/b811640g>.
- [97] Lindhoud S, Voorhaar L, de Vries R, Schweins R, Stuart MAC, Norde W. Salt-induced disintegration of lysozyme-containing polyelectrolyte complex micelles. *Langmuir* 2009;25:11425–30. <http://dx.doi.org/10.1021/la901591p>.
- [98] Lindhoud S, de Vries R, Norde W, Cohen Stuart MA. Structure and stability of complex coacervate core micelles with lysozyme. *Biomacromolecules* 2007;8:2219–27. <http://dx.doi.org/10.1021/bm0700688>.
- [99] Menger FM, Sykes BM. Anatomy of a coacervate. *Langmuir* 1998;14:4131–7.
- [100] Koga S, Williams DS, Perriman AW, Mann S. Peptide–nucleotide microdroplets as a step towards a membrane-free protocell model. *Nat Chem* 2011;3:720–4. <http://dx.doi.org/10.1038/nchem.1110>.
- [101] Cohen Stuart MA, Besseling NAM, Fokkink RG. Formation of micelles with complex coacervate cores. *Langmuir* 1998;14:6846–9. <http://dx.doi.org/10.1021/la980778m>.
- [102] Harada A, Kataoka K. Formation of polyion complex micelles in an aqueous milieu from a pair of oppositely-charged block copolymers with poly (ethylene glycol) segments. *Macromolecules* 1995;28:5294–9.
- [103] Tekaat M, Bütgerger D, Schönhoff M, Fery A, Cramer C. Scaling properties of the shear modulus of polyelectrolyte complex coacervates: a time–pH superposition principle. *Phys Chem Chem Phys* 2015;17:22552–6. <http://dx.doi.org/10.1039/C5CP02940F>.
- [104] Rawat K, Bohidar HB. Coacervation in Biopolymers. *J Phys Chem Biophys* 2014;4:1000165. <http://dx.doi.org/10.4172/2161-0398.1000165>.
- [105] Obermeyer AC, Mills CE, Dong X-H, Flores RJ, Olsen BD. Complex coacervation of supercharged proteins with polyelectrolytes. *Soft Matter* 2016;12:3570–81. <http://dx.doi.org/10.1039/C6SM00002A>.
- [106] Aumiller Jr WM, Keating CD. Phosphorylation-mediated RNA/peptide complex coacervation as a model for intracellular liquid organelles. *Nat Chem* 2016;8:129–37. <http://dx.doi.org/10.1038/nchem.2414>.
- [107] van der Kooij HM, Spruijt E, Voets IK, Fokkink R, Cohen Stuart MA, van der Gucht J. On the stability and morphology of complex coacervate core micelles: from spherical to wormlike micelles. *Langmuir* 2012;28:14180–91. <http://dx.doi.org/10.1021/la303211b>.
- [108] Flanagan SE, Malanowski AJ, Kizilay E, Seeman D, Dubin PL, Donato-Capel L, et al. Complex equilibria, speciation, and heteroprotein coacervation of lactoferrin and  $\beta$ -lactoglobulin. *Langmuir* 2015;31:1776–83. <http://dx.doi.org/10.1021/la504020e>.
- [109] Spruijt E, Sprakel J, Cohen Stuart MA, van der Gucht J. Interfacial tension between a complex coacervate phase and its coexisting aqueous phase. *Soft Matter* 2010;6:172–8. <http://dx.doi.org/10.1039/b911541b>.
- [110] Black KA, Piffitis D, Perry SL, Yip J, Byun WY, Tirrell M. Protein Encapsulation via Polypeptide Complex Coacervation. *ACS Macro Lett* 2014;3:1088–91. <http://dx.doi.org/10.1021/mz500529v>.
- [111] Spruijt E, Sprakel J, Lemmers M, Stuart MAC, van der Gucht J. Relaxation dynamics at different time scales in electrostatic complexes: time–salt superposition. *Phys Rev Lett* 2010;105:208301. <http://dx.doi.org/10.1103/PhysRevLett.105.208301>.
- [112] Dubin PL, Li Y, Jaeger W. Mesophase separation in polyelectrolyte–mixed micelle coacervates. *Langmuir* 2008;24:4544–9. <http://dx.doi.org/10.1021/la702405d>.
- [113] Dubin PL, Gao J, Mattison K. Protein purification by selective phase separation with polyelectrolytes. *Sep Purif Methods* 1994;23:1–16.
- [114] Xu Y, Mazzawi M, Chen K, Sun L, Dubin PL. Protein purification by polyelectrolyte coacervation: influence of protein charge anisotropy on selectivity. *Biomacromolecules* 2011;12:1512–22. <http://dx.doi.org/10.1021/bm101465y>.
- [115] Kayitmazer AB, Bohidar HB, Mattison KW, Bose A, Sarkar J, Hashidzume A, et al. Mesophase separation and probe dynamics in protein–polyelectrolyte coacervates. *Soft Matter* 2007;3:1064–76. <http://dx.doi.org/10.1039/b701334e>.
- [116] Kayitmazer AB, Quinn B, Kimura K, Ryan GL, Tate AJ, Pink DA, et al. Protein specificity of charged sequences in polyanions and heparins. *Biomacromolecules* 2010;11:3325–31. <http://dx.doi.org/10.1021/bm1008074>.
- [117] Macosko CW. *Rheology Principles, Measurements, and Applications*. VCH Publishers Inc; 1994.
- [118] Ferry JD. *Viscoelastic Properties of Polymers*. 3rd ed. John Wiley & Sons, Inc.; 1980.
- [119] Bird RB, Armstrong RC, Hassager O. *Dynamics of Polymeric Liquids*. vol. 1. John Wiley & Sons Inc.; 1987.
- [120] Morrison FA. *Understanding Rheology*. Oxford University Press; 2001.
- [121] Hyun K, Wilhelm M, Klein CO, Cho KS, Nam JG, Ahn KH, et al. A review of nonlinear oscillatory shear tests: analysis and application of large amplitude oscillatory shear (LAOS). *Prog Polym Sci* 2011;36:1697–753. <http://dx.doi.org/10.1016/j.progpolymsci.2011.02.002>.
- [122] Winter HH, Chambon F. Analysis of linear viscoelasticity of a crosslinking polymer at the gel point. *J Rheol* 1986;30:367–82.
- [123] Winter HH. Glass transition as the rheological inverse of gelation. *Macromolecules* 2013;46:2425–32. <http://dx.doi.org/10.1021/ma400086v>.
- [124] Hone JHE, Howe AM, Cosgrove T. A rheological and small-angle neutron scattering study of the structure of gelatin/polyelectrolyte complexes under shear. *Macromolecules* 2000;33:1199–205. <http://dx.doi.org/10.1021/ma991174x>.
- [125] Arfin N, Bohidar HB. Condensation, complex coacervation, and overcharging during DNA–gelatin interactions in aqueous solutions. *J Phys Chem B* 2012;116:13192–9. <http://dx.doi.org/10.1021/jp3073798>.
- [126] Boral S, Bohidar HB. Effect of ionic strength on surface-selective patch binding-induced phase separation and coacervation in similarly charged gelatin–agar molecular systems. *J Phys Chem B* 2010;114:12027–35. <http://dx.doi.org/10.1021/jp105431t>.
- [127] Chollakup R, Smithipong W, Eisenbach CD, Tirrell M. Phase behavior and coacervation of aqueous poly(acrylic acid)–poly(allylamine) solutions. *Macromolecules* 2010;43:2518–28. <http://dx.doi.org/10.1021/ma902144k>.
- [128] Chollakup R, Beck JB, Dirnberger K, Tirrell M, Eisenbach CD. Polyelectrolyte molecular weight and salt effects on the phase behavior and coacervation of aqueous solutions of poly(acrylic acid) sodium salt and poly(allylamine) hydrochloride. *Macromolecules* 2013;46:2376–90. <http://dx.doi.org/10.1021/ma202172q>.
- [129] Cousin F, Gummel J, Combet S, Boué F. The model lysozyme–PSSNa system for electrostatic complexation: similarities and differences with complex coacervation. *Adv Colloid Interface Sci* 2011;167:14. <http://dx.doi.org/10.1016/j.cis.2011.05.007>.
- [130] Espinosa-Andrews H, Enriquez-Ramírez KE, García-Márquez E, Ramírez-Santiago C, Lobato-Calleros C, Vernon-Carter J. Interrelationship between the zeta potential and viscoelastic properties in coacervates complexes. *Carbohydr Polym* 2013;95:161–6. <http://dx.doi.org/10.1016/j.carbpol.2013.02.053>.
- [131] Kaibara K, Okazaki T, Bohidar HB, Dubin PL. pH-induced coacervation in complexes of bovine serum albumin and cationic polyelectrolytes. *Biomacromolecules* 2000;1:100–7. <http://dx.doi.org/10.1021/bm990006k>.
- [132] Karimi F, Qazvini NT, Namivandi-Zangeneh R. Fish gelatin/laponite biohybrid elastic coacervates: a complexation kinetics–structure relationship study. *Int J Biol Macromol* 2013;61:102–13. <http://dx.doi.org/10.1016/j.jbiomac.2013.06.054>.
- [133] Mjahed H, Voegel JC, Chassepot A, Senger B, Schaaf P, Boulmedais F, et al. Turbidity diagrams of polyanion/polycation complexes in solution as a potential tool to predict the occurrence of polyelectrolyte multilayer deposition. *J Colloid Interface Sci* 2010;346:163–71. <http://dx.doi.org/10.1016/j.jcis.2010.02.042>.
- [134] Nigen M, Croguennec T, Bouhallab S. Formation and stability of  $\alpha$ -lactalbumin–lysozyme spherical particles: involvement of electrostatic forces. *Food Hydrocolloids* 2009;23:510–8. <http://dx.doi.org/10.1016/j.foodhyd.2008.02.005>.
- [135] Ogawa K. Effects of salt on intermolecular polyelectrolyte complexes formation between cationic microgel and polyanion. *Adv Colloid Interface Sci* 2015;226:115–21. <http://dx.doi.org/10.1016/j.cis.2015.09.005>.
- [136] Pathak J, Rawat K, Bohidar HB. Is surface patch binding between proteins symmetric about isoelectric pH? *RSC Adv* 2014;4:24710. <http://dx.doi.org/10.1039/c4ra02372b>.
- [137] Rawat K, Aswal VK, Bohidar HB. DNA–gelatin complex coacervation, UCST and first-order phase transition of coacervate to anisotropic ion gel in 1-methyl-3-octylimidazolium chloride ionic liquid solutions. *J Phys Chem B* 2012;116:14805–16. <http://dx.doi.org/10.1021/jp3102089>.
- [138] Ru Q, Wang Y, Lee J, Ding Y, Huang Q. Turbidity and rheological properties of bovine serum albumin/pectin coacervates: effect of salt concentration and initial protein/poly-saccharide ratio. *Carbohydr Polym* 2012;88:838–46.
- [139] Sanchez C, Mekhloufi G, Schmitt C, Renard D, Robert P, Lehr CM, et al. Self-assembly of  $\beta$ -lactoglobulin and acacia gum in aqueous solvent: structure and phase-ordering kinetics. *Langmuir* 2002;18:10323–33. <http://dx.doi.org/10.1021/la0262405>.
- [140] Sato H, Nakajima A. Complex coacervation in sulfated polyvinyl alcohol–aminoacetylated polyvinyl alcohol system. *Colloid Polym Sci* 1974;252:944–8. <http://dx.doi.org/10.1007/BF01566615>.
- [141] Tiwari A, Bindal S, Bohidar HB. Kinetics of protein–protein complex coacervation and bi-phasic release of salbutamol sulfate from coacervate matrix. *Biomacromolecules* 2009;10:184–9. <http://dx.doi.org/10.1021/bm801160s>.
- [142] Wang L, Cao Y, Zhang K, Fang Y, Nishinari K, Phillips GO. Hydrogen bonding enhances the electrostatic complex coacervation between K-carrageenan and gelatin. *Colloids Surf, A* 2015;482:604–10. <http://dx.doi.org/10.1016/j.colsurfa.2015.07.011>.
- [143] Weinbreck F, de Vries R, Schrooyen P, de Kruijff CG. Complex coacervation of whey proteins and gum Arabic. *Biomacromolecules* 2003;4:293–303. <http://dx.doi.org/10.1021/bm025667n>.
- [144] Weinbreck F, Rollema HS, Tromp RH, de Kruijff CG. Diffusivity of whey protein and gum Arabic in their coacervates. *Langmuir* 2004;20:6389–95. <http://dx.doi.org/10.1021/la049908j>.
- [145] Xia J, Dubin PL, Morishima Y, Sato T, Muhoberac BB. Quasielastic light scattering, electrophoresis, and fluorescence studies of lysozyme–poly(2-acrylamido–methylpropylsulfate) complexes. *Biopolymers* 1995;35:411–8. <http://dx.doi.org/10.1002/bip.360350408>.
- [146] Xu AY, Melton LD, Jameson GB, Williams MAK, McGillivray DJ. Structural mechanism of complex assemblies: characterisation of beta-lactoglobulin and pectin interactions. *Soft Matter* 2015;11:6790–9. <http://dx.doi.org/10.1039/C5SM01378J>.
- [147] Zhang Y, Yildirim E, Antila HS, Valenzuela LD, Sammalkorpi M, Lutkenhaus JL. The influence of ionic strength and mixing ratio on the colloidal stability of PDAC/PSS polyelectrolyte complexes. *Soft Matter* 2015;11:7392–401. <http://dx.doi.org/10.1021/acs.csm.5b09010>.
- [148] Webster L, Huglin MB, Robb ID. Complex formation between polyelectrolytes in dilute aqueous solution. *Polymer* 1997;38:1373–80.
- [149] Seyrek E, Dubin PL, Henriksen J. Nonspecific electrostatic binding characteristics of the heparin–antithrombin interaction. *Biopolymers* 2007;86:249–59. <http://dx.doi.org/10.1002/bip.20731>.
- [150] Prata AS, Grosso CRF. Influence of the oil phase on the microencapsulation by complex coacervation. *J Am Oil Chem Soc* 2015;92:1063–72. <http://dx.doi.org/10.1007/s11746-015-2670-z>.
- [151] Laaser JE, Jiang Y, Petersen SR, Reineke TM, Lodge TP. Interpolyelectrolyte Complexes of Polycationic Micelles and Linear Polyanions: Structural Stability and Temporal Evolution. *J Phys Chem B* 2015;119:15919–28. <http://dx.doi.org/10.1021/acs.jpcc.5b09010>.
- [152] Hirt S, Jones OG. Effects of chloride, thiocyanate and sulphate salts on  $\beta$ -lactoglobulin–pectin associative complexes. *Int J Food Sci Technol* 2014;49:2391–8. <http://dx.doi.org/10.1111/ijfs.12560>.
- [153] Dautzenberg F, Karibayants N. Polyelectrolyte complex formation in highly aggregating systems. Effect of salt: response to subsequent addition of NaCl. *Macromol Chem Phys* 1999;200:118–25. [http://dx.doi.org/10.1002/\(SICI\)1521-3935\(19990101\)200:1<118::AID-MACP118>3.0.CO;2-K](http://dx.doi.org/10.1002/(SICI)1521-3935(19990101)200:1<118::AID-MACP118>3.0.CO;2-K).
- [154] Boustma M, Leclercq L, Vert M, Vasilevska VV. Experimental and theoretical studies of polyanion–polycation complexation in salted media in the context of nonviral gene transfection. *Macromolecules* 2014;47:3574–81. <http://dx.doi.org/10.1021/ma500447k>.

- [155] Salehi A, Desai PS, Li J, Steele CA, Larson RG. Relationship between polyelectrolyte bulk complexation and kinetics of their layer-by-layer assembly. *Macromolecules* 2015;48:400–9. <http://dx.doi.org/10.1021/ma502273a>.
- [156] Burgess DJ. Practical analysis of complex coacervate systems. *J Colloid Interface Sci* 1990;140:227–38. [http://dx.doi.org/10.1016/0021-9797\(90\)90338-O](http://dx.doi.org/10.1016/0021-9797(90)90338-O).
- [157] Wang Q, Schlenoff JB. The polyelectrolyte complex/coacervate continuum. *Macromolecules* 2014;47:3108–16. <http://dx.doi.org/10.1021/ma500500q>.
- [158] Seyrek E, Dubin PL, Tribet C, Gamble EA. Ionic strength dependence of protein–polyelectrolyte interactions. *Biomacromolecules* 2003;4:273–82. <http://dx.doi.org/10.1021/bm025664a>.
- [159] Dautzenberg H, Jaeger W. Effect of charge density on the formation and salt stability of polyelectrolyte complexes. *Macromol Chem Phys* 2002;203:2095–102.
- [160] Kabanov V. Fundamentals of polyelectrolyte complexes in solution and the bulk. In: Decher G, Schlenoff JB, editors. *Multilayer thin films: sequential assembly of nanocomposite materials*. New York: Wiley; 2003. p. 47–86.
- [161] Weinbreck F, Nieuwenhuijse H, Robijn GW, de Kruijff CG. Complexation of whey proteins with carrageenan. *J Agric Food Chem* 2004;52:3550–5. <http://dx.doi.org/10.1021/jf034969t>.
- [162] Zhang L, Lipik V, Miserez A. Complex coacervates of oppositely charged co-polypeptides inspired by the sandcastle worm glue. *J Mater Chem B* 2016;4:1544–56. <http://dx.doi.org/10.1039/C5TB02298C>.
- [163] Overbeek JTG, Vroom MJ. Phase separation in polyelectrolyte solutions. Theory of complex coacervation. *J Cell Comp Physiol* 1957;49:7–26. <http://dx.doi.org/10.1002/jcp.1030490404>.
- [164] Jha P, Desai P, Li J, Larson R. pH and salt effects on the associative phase separation of oppositely charged polyelectrolytes. *Polymers* 2014;6:1414–36. <http://dx.doi.org/10.3390/polym6051414>.
- [165] Qin J, Priftis D, Farina R, Perry SL, Leon L, Whitmer JK, et al. Interfacial tension of polyelectrolyte complex coacervate phases. *ACS Macro Lett* 2014;3:565–8. <http://dx.doi.org/10.1021/mz500190w>.
- [166] Perry SL, Sing CE. PRISM-based theory of complex coacervation: excluded volume versus chain correlation. *Macromolecules* 2015;48:5040–53. <http://dx.doi.org/10.1021/acs.macromol.5b01027>.
- [167] Tainaka K-I. Effect of counterions on complex coacervation. *Biopolymers* 1980;19:1289–98. <http://dx.doi.org/10.1002/bip.1980.360190705>.
- [168] Veis A. A review of the early development of the thermodynamics of the complex coacervation phase separation. *Adv Colloid Interface Sci* 2011;167:2–11. <http://dx.doi.org/10.1016/j.cis.2011.01.007>.
- [169] Biesheuvel PM, Cohen Stuart MA. Electrostatic free energy of weakly charged macromolecules in solution and intermacromolecular complexes consisting of oppositely charged polymers. *Langmuir* 2004;20:2785–91. <http://dx.doi.org/10.1021/la036204l>.
- [170] Sing CE. Development of the modern theory of polymeric complex coacervation. *Adv Colloid Interface Sci* 2016. <http://dx.doi.org/10.1016/j.cis.2016.04.004> [(inpress)].
- [171] Momeni A, Filiaggi MJ. Rheology of polyphosphate coacervates. *J Rheol* 2016;60:25–34. <http://dx.doi.org/10.1122/1.4935127>.
- [172] Liberatore MW, Wyatt NB, Henry M, Dubin PL, Foun E. Shear-induced phase separation in polyelectrolyte/mixed micelle coacervates. *Langmuir* 2009;25:13376–83. <http://dx.doi.org/10.1021/la903260r>.
- [173] Gupta AN, Bohidar HB, Aswal VK. Surface patch binding induced intermolecular complexation and phase separation in aqueous solutions of similarly charged gelatin–chitosan molecules. *J Phys Chem B* 2007;111:10137–45. <http://dx.doi.org/10.1021/jp070745s>.
- [174] Weinbreck F, Wientjes RHW, Nieuwenhuijse H, Robijn GW, de Kruijff CG. Rheological properties of whey protein/gum Arabic coacervates. *J Rheol* 2004;48:1215–28. <http://dx.doi.org/10.1122/1.1795191>.
- [175] Mohanty B, Aswal VK, Kohlbrecher J, Bohidar HB. Length scale hierarchy in sol, gel, and coacervate phases of gelatin. *J Polym Sci B* 2006;44:1653–67. <http://dx.doi.org/10.1002/polb.20783>.
- [176] Gupta RK. *Polymer and composite rheology*. 2nd ed. Marcel Dekker, Inc.; 2000
- [177] Arfin N, Aswal VK, Bohidar HB. Overcharging, thermal, viscoelastic and hydration properties of DNA–gelatin complex coacervates: pharmaceutical and food industries. *RSC Adv* 2014;4:11705–13. <http://dx.doi.org/10.1039/C3RA46618C>.
- [178] Qazvini NT, Bolisetty S, Adamcik J, Mezzenga R. Self-healing fish gelatin/sodium montmorillonite biohybrid coacervates: structural and rheological characterization. *Biomacromolecules* 2012;13:2136–47. <http://dx.doi.org/10.1021/bm3005319>.
- [179] Rocha CMR, Souza HKS, Magalhães NF, Andrade CT, Gonçalves MP. Rheological and structural characterization of agar/whey proteins insoluble complexes. *Carbohydr Polym* 2014;110:345–53.
- [180] Wang X, Lee J, Wang Y-W, Huang Q. Composition and rheological properties of  $\beta$ -lactoglobulin/pectin coacervates: effects of salt concentration and initial protein/polysaccharide ratio. *Biomacromolecules* 2007;8:992–7.
- [181] Spruijt E, van den Berg SA, Cohen Stuart MA, van der Gucht J. Direct measurement of the strength of single ionic bonds between hydrated charges. *ACS Nano* 2012;6:5297–303. <http://dx.doi.org/10.1021/nn301097y>.
- [182] Pathak J, Rawat K, Bohidar HB. Charge heterogeneity induced binding and phase stability in  $\beta$ -lacto-globulin–gelatin B gels and coacervates at their common pl. *RSC Adv* 2015;5:67066–76. <http://dx.doi.org/10.1039/C5RA07195j>.
- [183] Winter HH. Can the gel point of a cross-linking polymer be detected by the G'–G'' crossover? *Polym Eng Sci* 1987;27:1698–702. <http://dx.doi.org/10.1002/pen.760272209>.
- [184] Krogstad DV, Lynd NA, Miyajima D, Gopez J, Hawker CJ, Kramer EJ, et al. Structural evolution of polyelectrolyte complex core micelles and ordered-phase bulk materials. *Macromolecules* 2014;47:8026–32. <http://dx.doi.org/10.1021/ma5017852>.
- [185] Krogstad DV, Choi S-H, Lynd NA, Audus DJ, Perry SL, Gopez JD, et al. Small angle neutron scattering study of complex coacervate micelles and hydrogels formed from ionic diblock and triblock copolymers. *J Phys Chem B* 2014;118:13011–8. <http://dx.doi.org/10.1021/jp509175a>.
- [186] Krogstad DV. *Investigating the structure–property relationships of aqueous self-assembled materials*. University of California at Santa Barbara; 2012.
- [187] Koide A, Kishimura A, Osada K, Jang W-D, Yamasaki Y, Kataoka K. Semipermeable polymer vesicle (PICsome) self-assembled in aqueous medium from a pair of oppositely charged block copolymers: physiologically stable micro-/nancontainers of water-soluble macromolecules. *J Am Chem Soc* 2006;128:5988–9. <http://dx.doi.org/10.1021/ja057993r>.
- [188] Kishimura A, Koide A, Osada K, Yamasaki Y, Kataoka K. Encapsulation of myoglobin in PEGylated polyion complex vesicles made from a pair of oppositely charged block ionomers: a physiologically available oxygen carrier. *Angew Chem Int Ed* 2007;46:6085–8. <http://dx.doi.org/10.1002/anie.200701776>.
- [189] Lemmers M, Sprakel J, Voets IK, van der Gucht J, Stuart MAC. Multiresponsive reversible gels based on charge-driven assembly. *Angew Chem Int Ed* 2010;49:708–11. <http://dx.doi.org/10.1002/anie.200905515>.
- [190] Elbaum-Garfinkle S, Kim Y, Szczepaniak K, Chen CC-H, Eckmann CR, Myong S, et al. The disordered P granule protein LAF-1 drives phase separation into droplets with tunable viscosity and dynamics. *Proc Natl Acad Sci U S A* 2015;201504822. <http://dx.doi.org/10.1073/pnas.1504822112>.
- [191] Fuller GM. *Optical rheometry of complex fluids*. Oxford University Press; 1995.
- [192] Niang PM, Huang Z, Dulong V, Souguir Z, Le Cerf D, Picton L. Thermo-controlled rheology of electro-assembled polyanionic polysaccharide (alginate) and polycationic thermosensitive polymers. *Carbohydr Polym* 2016;139:67–74. <http://dx.doi.org/10.1016/j.carbpol.2015.12.022>.
- [193] Ortony JH, Hwang DS, Franck JM, Waite JH, Han S. Asymmetric collapse in biomimetic complex coacervates revealed by local polymer and water dynamics. *Biomacromolecules* 2013;14:1395–402. <http://dx.doi.org/10.1021/bm4000579>.
- [194] Huang GQ, Xiao JX, Wang SQ, Qiu HW. Rheological properties of O-carboxymethyl chitosan – gum Arabic coacervates as a function of coacervation pH. *Food Hydrocolloids* 2015;43:436–41. <http://dx.doi.org/10.1016/j.foodhyd.2014.06.015>.
- [195] Schaaf P, Schlenoff JB. Saloplastics: processing compact polyelectrolyte complexes. *Adv Mater* 2015;27:2420–32. <http://dx.doi.org/10.1002/adma.201500176>.
- [196] Sánchez VE, Bartholomai GB, Pilosof AMR. Rheological properties of food gums as related to their water binding-capacity and to soy protein–interaction. *Lebensm-Wiss Technol* (1968–2004) 1995;28:380–5.